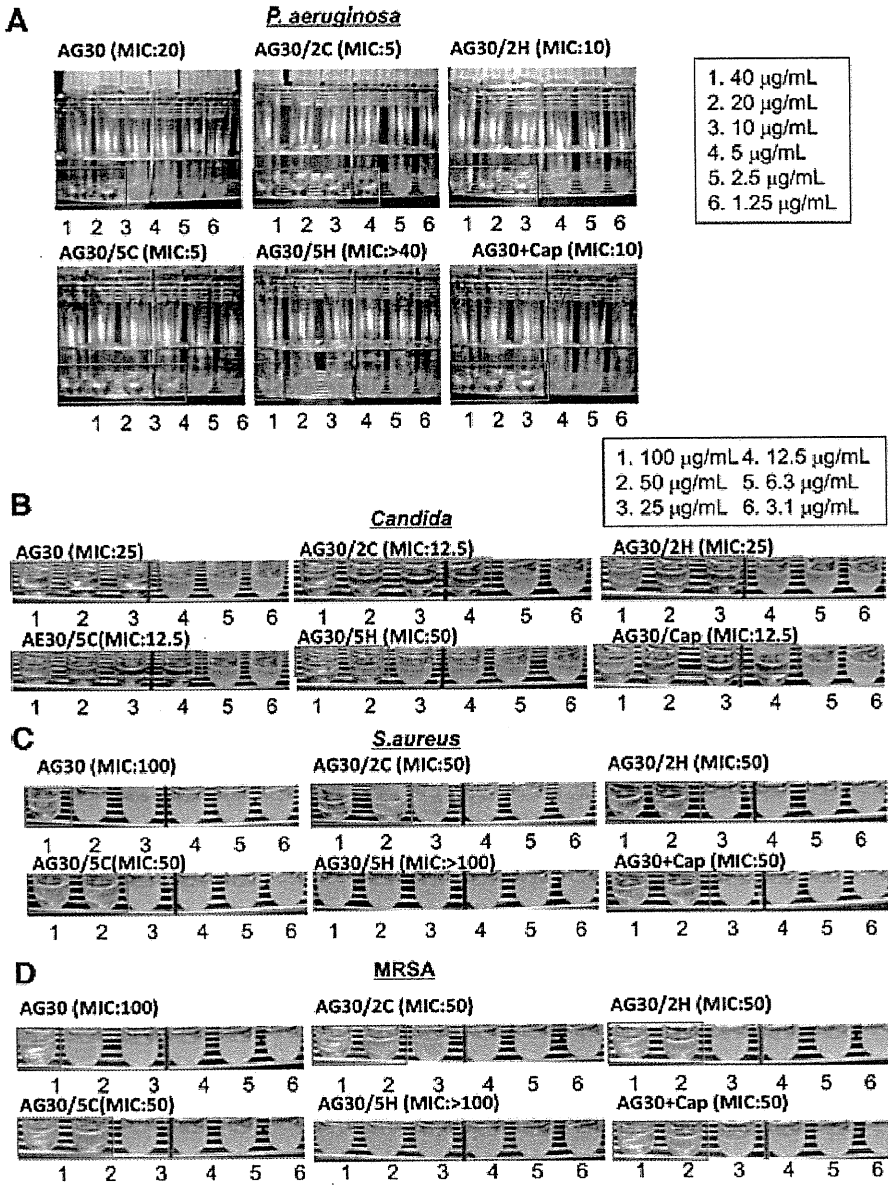

Fig. 2 The antibacterial action of modified AG30. The antibacterial action of modified AG30 is evaluated to (**A**) *P. aeruginosa* (ATCC27853), (**B**) *Candida* (ATCC90028), (**C**) *S. aureus* (ATCC29213) and (**D**) MRSA. MIC assays were performed in the concentration range of 1.25–40 mg/ml of modified AG30, LL37 against *P. aeruginosa* and 3.1–100 mg/ml against *Candida*, *S. aureus* and MRSA. MIC was defined as the lowest peptide concentration, which prevented visible bacterial growth in the medium. Lower panel shows representative pictures of MIC assays with treatment of several peptides.

antibacterial effects might occur through a 'lytic' mechanism that results from the attachment of cationic peptides to the bacterial membrane. To test this idea, we exogenously added cationic ions, such as $CaCl_2$ or $MgCl_2$, and examined whether the antibacterial effect of AG30/5C was inhibited. Indeed, the addition of $CaCl_2$ or $MgCl_2$ (both at 3 and 6 mM) completely blocked the antibacterial effects of AG30/5C (Table 2). These results suggest that AG30/5C kills bacteria through a lysis-based mechanism that may be different from the actions of other antibiotics.

Based on these results, we selected molecules to which five cationic amino acids has been added (*i.e.* compound AG30/5C) as lead compounds for the next stage of investigation and further evaluated the function of AG30/5C.

Development of a production system for modified AG30 (AG30/5C)

To facilitate the eventual clinical investigation/application of these compounds, we developed a large-scale procedure for the synthesis of AG30/5C that employed the conventional solution method and met Good Manufacturing Practice guidelines. The AG30/5C molecule was assembled from four segments, that is (1–10), (11–17), (18–23) and (24–30), as shown in Figure 4A. The carboxyl terminus of each of the segments was protected by a phenacyl ester (Pac) group, except for the C-terminal segment that was instead protected by a benzyl ester group. All of the side-chain functional groups were protected as follows:

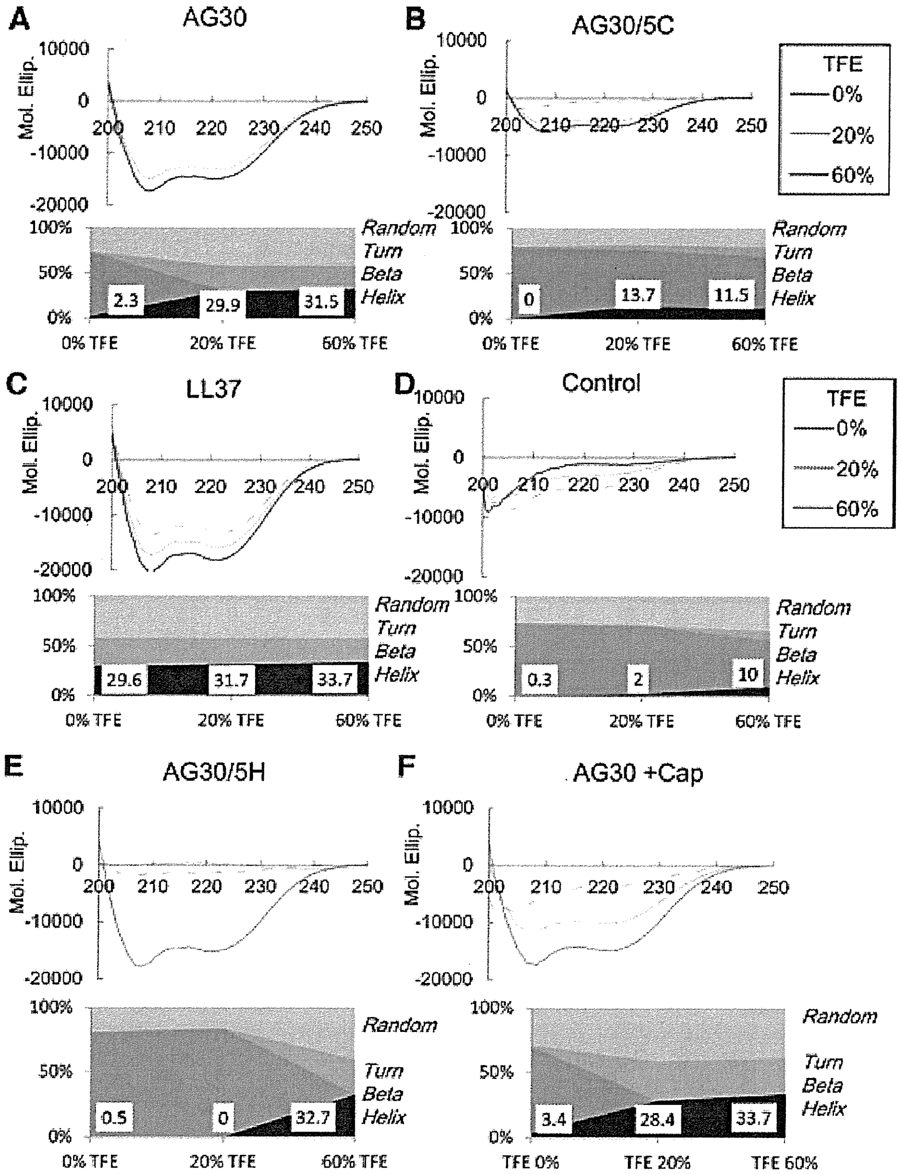

Fig. 3 CD spectroscopy analysis. Modified AG30, LL37 and control peptide showed negligible helical structure in aqueous buffer, and the addition of the helix inducing cosolvent trifluoroethanol (20% or 60%) resulted in the appearance of a clear helical component, that demonstrated the minimum at 208 and 220 nm and the increase of ellipticity at 200 nm. In lower panel, the quantification of helical structure (Random, Turn, Beta, and Helix) was calculated, and the score of helix has been shown.

2-chlorobenzyloxycarbonyl (ClZ) for Lys, benzyloxymethyl (Bom) for His, *p*-toluenesulfonyl (Tos) for Arg, formyl (CHO) for Trp and 2-bromobenzyloxycarbonyl (BrZ) for Tyr. Each segment was elongated stepwise using the EDC/HOBt coupling reagent method. During the chain assembly, the common starting material (*i.e.* Boc-Arg(Tos)-Leu-OPac) could be used for preparing segments (1–10), (11–17) and (18–23) because AG30/5C contains an Arg-Leu sequence at positions 9–10, 16–17 and 22–23. This facilitated the preparation of these segments. Before being subjected to segment condensation reactions, each segment was treated with zinc powder in acetic acid to remove the Pac group from the C-terminus. The C-terminal segment was elongated in a sequential manner with segments containing a free carboxylic acid at the C-terminus by applying the EDC/HOOBt method in DMF to obtain the fully protected AG30/5C peptide. After subsequent removal of the N^{α}-Boc group and the CHO group on Trp using TFA and 10% piperidine/DMF, all of the protecting groups were removed by HF/*p*-cresol (v/v, 85/15) in the presence of methoxyamine·HCl and 2-mercaptopyridine at −2°C to −5°C for 1 hr [17]. After conversion of the peptide from the HF form to the AcOH form using a Muromac (acetate form) column, the crude product was purified by ion-exchange chromatography on a CM-Sepharose column using a gradient of 20 mM $AcONH_4$ buffer to 2 M NaCl/20 mM $AcONH_4$ buffer (pH 5.0). This was followed by RP-HPLC on an YMC-Pak ODS column using a gradient of 20% CH_3CN/0.1% TFA to 40% CH_3CN/0.1% TFA. The purified product was passed

Table 1 MIC of AG30 or AG30/5C to antibiotics-resistant starain (A–E) of *P. aeruginosa*

	A	B	C	D	E
AG30	20	10	40	20	10
+5C	10	5	20	20	10
CAZ	<8: S	<8: S	<8: S	<8: S	>32: R
CFPM	<8: S	<8: S	<8: S	<8: S	>16: R
CPZ	<16: S	32	<16: S	<16: S	>32: R
IPM/CS	<4: S	<4: S	<4: S	>8: R	<4: S
AZT	<8: S	>16: R	<8: S	<8: S	>16: R
TOB	>8: R	<4: S	>8: R	<4: S	<4: S
GM	>8: R	<4: S	>8: R	<4: S	8
FOM	>16: R	>16: R	>16: R	>16: R	>16: R
LVFX	<2: S	<2: S	<2: S	4: S	>4: R
CPFX	<1: S	<1: S	<1: S	<1: S	>2: R

The score shows MIC (mg/ml) for *P. aeruginosa* (A–E). R indicates resistance and S indicates sensitive to *P. aeruginosa*.
CAZ: ceftazidime hydrate; CFPM: cefepime hidrochloride hydrate; CPZ: cefoperazone sodium; IPM/CS: imipenem/cilastatin sodium; AZT: aztreonam; TOB: tobramycin; GM: Gentamicin sulfate; FOM: fosfomycin sodium; LVFX: levofloxacin hydrate; CPFX: Ciprofloxacin hydrochloride.

Table 2 Effect of cationic ions or FBS on MIC of AG30 or AG30/5C to *P. aeruginosa*

	AG30	AG30/5C
No treat	20	5
+1 mM $MgCl_2$	80	20
+3 mM $MgCl_2$	>80: R	>80: R
+6 mM $MgCl_2$	>80: R	>80: R
+1 mM $CaCl_2$	40	20
+3 mM $CaCl_2$	>80: R	>80: R
+6 mM $CaCl_2$	>80: R	>80: R
+10% FBS	>80:R	>80:R

The score shows MIC (mg/ml) for *P. aeruginosa*. R indicates resistance to *P. aeruginosa* (ATCC27853).
FBS: foetal bovine serum.

successively through columns of Muromac (acetate form) and Sephadex G-10 using dilute acetic acid as an eluant, which was summarized in Figure 4B. We confirmed that the antibacterial and angiogenic functions of the peptides synthesized using the conventional solution method were similar to those synthesized by the previous solid method (data not shown). The advantages of this method include reduced synthesis cost and GMP grade applicability. Indeed, the cost to produce this peptide at a 10 g scale was roughly hundred thousand dollars, more than 10-fold reduction in price in comparison to the solid method. In addition, for GMP-scale procedures, each peptide-synthesis process is the same in the initial steps, and the final coupling reaction will be performed in the GMP facility. Based on this method, we will commence with large-scale production of this peptide for use in clinical trials.

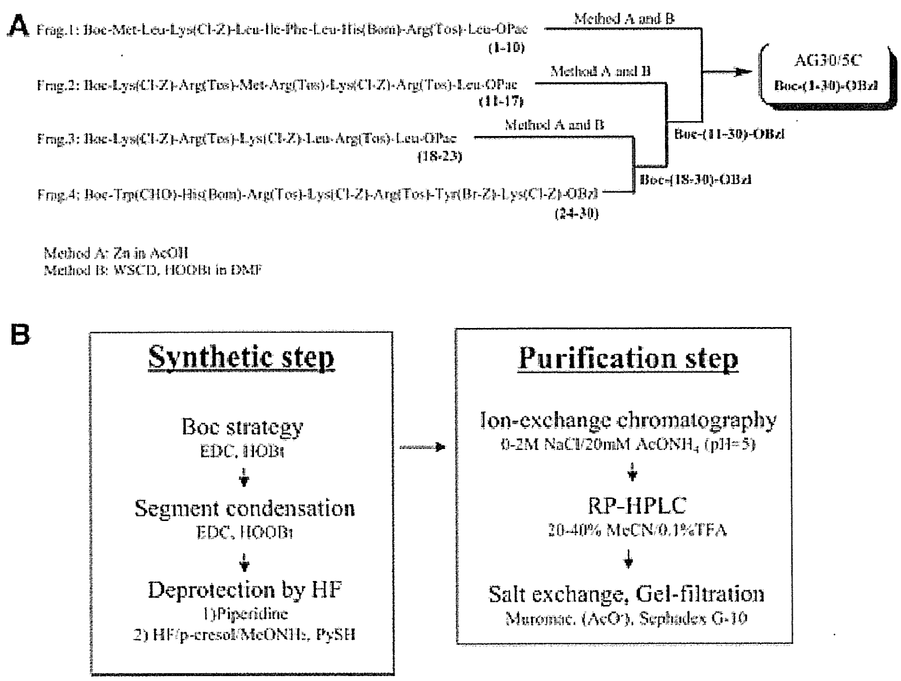

Fig. 4 The scheme for the synthesis of AG30/5C. (**A**) The AG30/5C molecule was assembled from four segments, that is (1–10), (11–17), (18–23) and (24–30), and each segment was elongated stepwise using the EDC/HOBt method as coupling reagents. (**B**) A large-scaled procedure employing the conventional solution method that is applicable for Good Manufacturing Practice toward clinical application in both synthetic and purification steps. The crude product was purified by ion-exchange chromatograpy followed by RP-HPLC. The purified product was passed successively through columns of Muromac and Sephadex G-10.

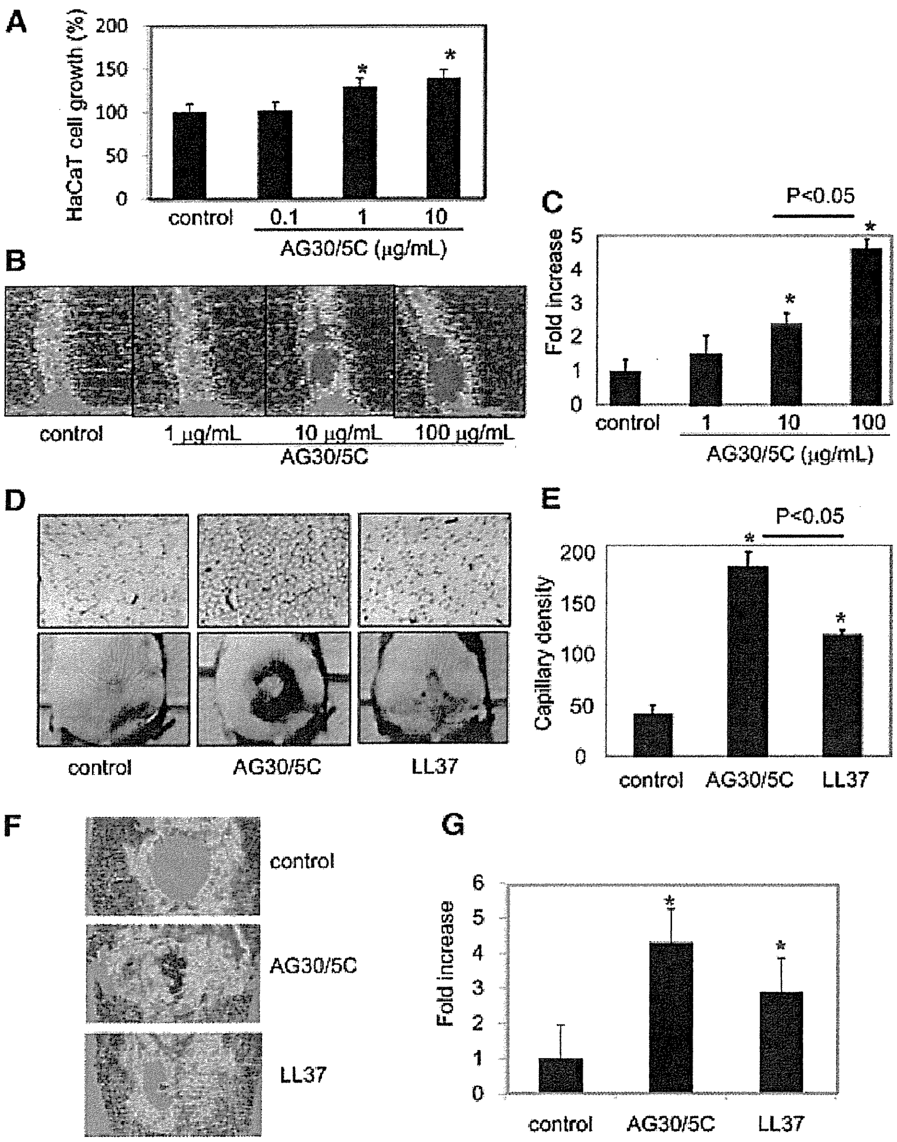

Fig. 5 Evaluation of the angiogenic effects of AG30/5C in a wound-healing model. (**A**) Cell growth of HaCaT cells in the presence of AG30/5C (0, 0.1, 1 and 10 μg/ml). The quantification is presented as a percent increase. $N = 8$ per group and duplicated. (**B**, **C**) Blood flow was analysed by Laser Doppler Image in mouse tails 3 days after induction of full thickness injuries with topical application of AG30/5C (0, 1, 10 and 100 μg/ml). Low or no perfusion is displayed as dark blue, whereas the highest perfusion interval is displayed as red; the quantification is presented as a fold increase. $N = 3$–5 per group and duplicated. $*P < 0.05$ *vs.* control. (**D**, **E**) Evaluation of wound healing in a diabetic mouse model treated with saline (control), AG30/5C or LL37. (**D**) The upper panel shows representative immunostains using anti-CD31 (PECAM) antibody (brown). The lower panel shows representative pictures after wound closure (day 24). Hair growth was observed around the edge of wound. (**E**) Capillary densities were quantified by cross section of ischaemic tissues immunostained with anti-CD31 (PECAM) antibody. $N = 6$–10 per group and duplicated. $*P < 0.05$ *vs.* control. (**F**) Blood flow was analysed by LDI in mouse wound 3 days after operation with topical application of AG30/5C (100 μg/ml). Low or no perfusion is displayed as grey or dark blue, whereas the highest perfusion interval is displayed as yellow or red; the quantification is presented as a fold increase. $N = 5$–6 per group and duplicated. $*P < 0.05$ *vs.* control.

We further examined the stability of this peptide in saline solution at both 5°C and room temperature. RP-HPLC analysis revealed that AG30/5C was fairly stable under 5°C for 12 months (96% stability), although it was less stable at room temperature (85% stability).

Effects of AG30/5C on murine and porcine wound models

In the process of wound healing, epidermal cell growth as well as angiogenesis is required to accelerate the time course of wound healing. Thus, we tested to examine the direct effect of AG30/5C on HaCaT cells. As shown in Figure 5A, the treatment of AG30/5C induced cell growth of HaCaT cells in a dose dependent manner. Thus, in the process of wound healing, AG30/5C can accelerate epithelialization as well as angiogenesis.

To evaluate the suitable dose of AG30/5C using a wound model [12], we measured the blood flow of mouse tails 3 days after inducing a full thickness injury. The topical application of AG30/5C at a dose of either 10 or 100 μg/ml significantly increased blood flow in a dose-dependent manner (Fig. 5B and C). Based on these results, we evaluated the angiogenic effects of AG30/5C and LL37 in a diabetic mouse wound-healing model. Capillary density within the ischaemic thigh adductor skeletal muscles was analysed to obtain specific evidence of vascularity at the level of the microcirculation [13, 14]. In the analysis of angiogenesis, microcapillary density was significantly increased

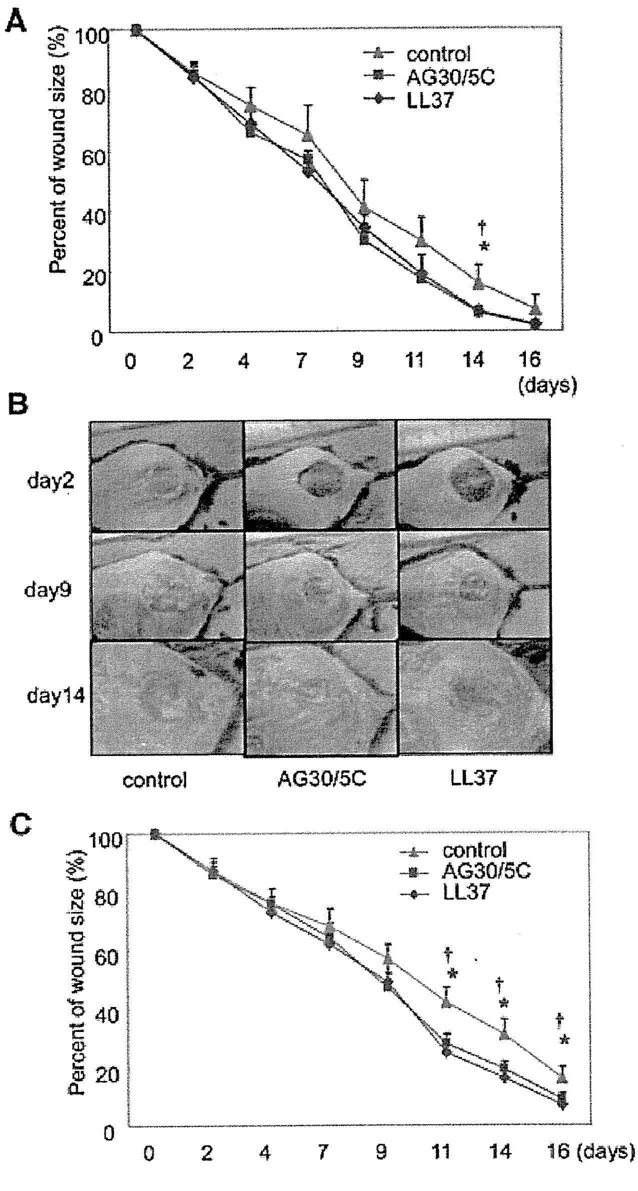

Fig. 6 Evaluation of the effects of AG30/5C in a diabetic mouse wound-healing model with or without MRSA infection. (**A**) Time course of the quantification of wound size in diabetic mice with treatment of saline (control), AG30/5C or LL37 (100 μg/ml, respectively). $N = 6–10$ per group and duplicated. $^{*}P < 0.05$ *vs.* AG30/5C, $^{\dagger}P < 0.05$ *vs.* LL37. (**B, C**) Evaluation of infectious wound healing in a diabetic mouse model treated with saline (control), modified AG30 or LL37. (**B**) Representative pictures of infectious wounds at days 2, 9 and 14. (**C**) Time course of the quantification of infectious wound size in diabetic mice treated with saline (control), AG30/5C or LL37 (100 μg/ml, respectively). $N = 5–9$ per group and duplicated. $^{*}P < 0.05$ *vs.* AG30/5C, $^{\dagger}P < 0.05$ *vs.* LL37.

in the AG30/5C-treated group in comparison to the LL37-treated group (Fig. 5D and E). Interestingly, at day 28 the hair growth was frequently observed in the AG30/5C-treated group (Fig. 5C). This result may support the angiogenic effects of AG30/5C because perifollicular angiogenesis undergoes a hair-cycle-dependent expansion and degeneration stage [20]. We further evaluated the angiogenic property of AG30/5C by measuring the blood flow just below the skin around wound. The evaluation of blood flow is also useful to examine an angiogenic effect [18]. As shown in Figure 5F and G, AG30/5C or LL37 treatment significantly increased the blood flow around the wound, compared with control group. These results illustrate the angiogenic properties of AG30/5C in wound-healing models.

Quantified analysis of the effect of AG30/5C in a wound-healing model

To investigate the possible clinical applications of AG30/5C, we quantified the effects of the peptide in a murine wound model. Under dressing conditions either with or without AG30/5C or LL37, the topical application of both compounds significantly decreased wound size at day 14 (Fig. 6A). Furthermore, three of the control-peptide-treated mice were afflicted with *S. aureus* infections during these experiments; in contrast, none of the mice in the AG30/5C- or LL37-treated groups became infected.

We also evaluated the antibacterial effects of AG30/5C using a murine infectious wound model. After topical treatment of MRSA on wounds, yellow pus was observed at day 2 and continuously increased over the duration of the experiment (Fig. 6B). We confirmed the presence of *S. aureus* in this yellow pus. Indeed, the infection delayed the time course of wound healing compared to a non-infectious wound-healing model. Importantly, co-treatment of either AG30/5C or LL37 attenuated the increase of yellow pus on the wounds (Fig. 6B) and significantly decreased wound size at days 11, 14 and 16 after treatment (Fig. 6C).

We further examined the effect of AG30/5C using a porcine wound model. After the topical application of both compounds every 2 days for 12 days under dressing condition, the diameter in the longitudinal views was evaluated as follows (control: 16.2 ± 0.5 mm, AG30/5C: 14.2 ± 0.5 mm, LL37: 15.4 ± 0.8 mm; Fig. 7A). In the evaluation of angiogenesis using a porcine wound model, microcapillary density was also significantly increased in both AG30/5C- and LL/37-treated groups in comparison to a control group (Fig. 7B and C). These results suggest that AG30/5C can potentially accelerate the wound-healing process.

Discussion

In this study, we modified a previously described functional peptide, AG30, in an effort to develop novel wound-healing drugs that could potentially be used for clinical applications. Historically, many microbial peptides have failed to prove effective in clinical applications; this is likely because such small peptides can be easily degraded by peptidases in addition to their short half-lives.

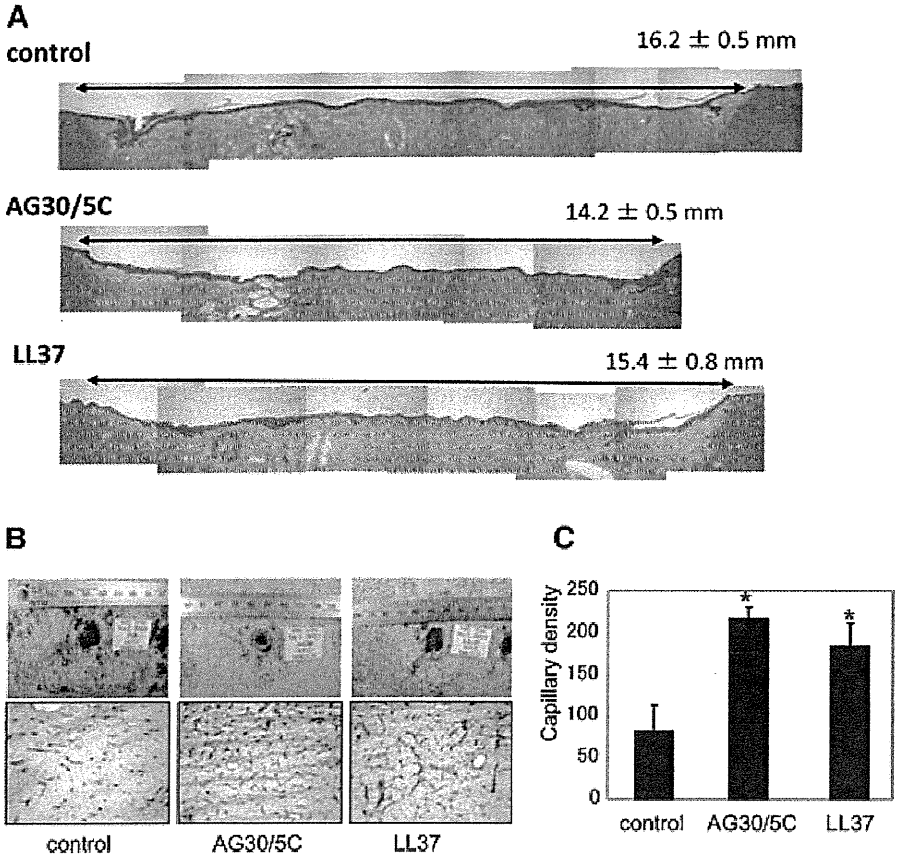

Fig. 7 Evaluation of the effects of AG30/5C on a porcine wound-healing model. (**A**) Representative pictures of H&E staining on full-thickness section with restored epithelium, treated with saline (control), AG30/5C or LL37 (100 μg/ml, respectively). In the upper right corner, means ± S.E.M. (mm) were shown. (**B**) The upper panel shows representative pictures of wound healing in each group (day 9). The lower panel shows representative immunostains using anti-vWF antibody (brown). (**C**) Capillary densities were quantified by cross section of ischaemic tissue immunostained with anti-vWF antibody. $*P < 0.05$ *vs.* control. N = 6 per group and duplicated.

This study is a follow-up to a previous feasibility study aimed at generating lead compounds from a foundation compound.

Short cationic amphipathic peptides with antimicrobial and/or immunomodulatory activities are important components of the innate immune response and provide a template for two separate classes of antimicrobial drugs. Rapid acting and potent antimicrobial peptides are promising targets for investigation in the development of clinical treatments. In our modifications of the foundation peptide, we addressed the net positive charge and the amphipathic three-dimensional structure of AG30, and designed to modulate the balance between a net charge and α-helical structure by replacing a few amino acids. As a result, AG30/5C, replaced of five cationic amino acids, exhibited increased angiogenic and antimicrobial activities. Although AG30/5C showed the lowest ratio of α-helical the structure is still helical, and the three-dimentional structure of AG30/5C showed the broad cationic peptide surface. Thus, we speculate that AG30/5C can keep the cationic surface, which leads to increased activity, even though α-helical structure is not tightly fixed. Balancing these two parameters, thus enabling the net positive charged surface to attach and accumulate at the cell surface, was critical for the activity of this peptide. Indeed, the antibacterial action of this peptide was antagonized by the addition of divalent cations such as Mg^{2+} and Ca^{2+}. Some studies have modified antimicrobial peptides to develop new classes of antibiotics; however, this is the first report to modulate both antibacterial and angiogenic actions while maintaining activity and structure. The strategies and methods presented here could be useful in the further modifications of potential peptides in the early stages of clinical development.

Cationic antimicrobial peptides have a mixed history in clinical trials. The cationic peptides polymixin B and gramicidin S have long been used both in the clinic and as topical over-the-counter medicines. However, despite several clinical trials over the past ten years, the clinical success of cationic antimicrobial peptides has been limited [20]. To date, four cationic peptides have advanced into phase-III clinical trials. These peptides have been designed for treating impetigo and diabetic foot ulcers (the frog magainin derivative MSI-78; Pexiganan), oral mucosaitis (the pigprotegrin derivative IB-367; Iseganan), sepsis (the human bactericidal permeability protein derivative $rBPI_{23}$; Neuprex) and catheter-associated infections (the cattle indolicidin variant CP-226; Omiganan). Among them, Omiganan has achieved statistically significant success both in reducing infections that tunnel in from the catheter insertion site and in reducing catheter colonization during phase IIa trials [21]. Importantly, all four peptides are derivatives that were generated from original cationic peptides. Thus, in this study, we employed a feasibility study to develop lead compounds. Using an animal wound-healing model, we utilized simple topical application without ointment or cream; this provided insight into the effectiveness of our peptide as a therapeutic drug and revealed some important limitations. To improve the effectiveness of the peptide as a therapeutic drug, it is possible that production of AG30/5C as an ointment or cream might enhance the local accumulation and structural stability of the peptide. The other aspect of peptide modification for eventual clinical development is to consider the cost of generating a peptide at the GMP level. In this study, we attempted to develop a large-scale procedure for the synthesis of AG30/5C that employed a conventional solution method applicable to Good Manufacturing Practice; importantly, we succeeded in generating a therapeutic peptide for use in pre-clinical trials. Furthermore, we tried to shorten the peptide while maintaining both its angiogenic and its antibacterial actions in an effort to minimize costs.

Based on these results, we have now transitioned into a pre-clinical study that includes evaluations of toxicity at single or repeated doses, genotoxicity and examination using local stimulation while monitoring serum concentrations of AG30/5C. We will continue to propose AG30/5C as a wound-healing drug for the treatment of ischaemic ulcers of diabetes patients or peripheral arterial diseases.

Acknowledgements

We thank all the members of the Gene Therapy Science Laboratory for critical discussions during the course of this work. We also thank Yuichi Koga and Kazufumi Takano in Department of Material and Life Science, Osaka University for technical help in CD analysis. This work was supported by the National Institute of Biomedical Innovation and the Takeda Science Foundation.

Conflict of interest

The authors declare no conflict of interest.

References

1. **Zasloff M.** Antimicrobial peptides of multicellular organisms. *Nature.* 2002; 415: 389–95.
2. **Hancock RE, Patrzykat A.** Clinical development of cationic antimicrobial peptides: from natural to novel antibiotics. *Curr Drug Targets Infect Disord.* 2002; 2: 79–83.
3. **Giangaspero A, Sandri L, Tossi A.** Amphipathic alpha helical antimicrobial peptides. *Eur J Biochem.* 2001; 268: 5589–600.
4. **Shai Y.** Mode of action of membrane active antimicrobial peptides. *Biopolymers.* 2002; 66: 236–48.
5. **Sorensen O, Bratt T, Johnsen AH, *et al.*** The human antibacterial cathelicidin, hCAP-18, is bound to lipoproteins in plasma. *J Biol Chem.* 1999; 274: 22445–51.
6. **Nishikawa T, Nakagami H, Maeda A, *et al.*** Development of a novel antimicrobial peptide, AG-30, with angiogenic properties. *J Cell Mol Med.* 2008; 13: 535–46.
7. **Rikitake Y, Hirata K, Kawashima S, *et al.*** Involvement of endothelial nitric oxide in sphingosine-1-phosphate-induced angiogenesis. *Arterioscler Thromb Vasc Biol.* 2002; 22: 108–14.
8. **Koczulla R, von Degenfeld G, Kupatt C, *et al.*** An angiogenic role for the human peptide antibiotic LL-37/hCAP-18. *J Clin Invest.* 2003; 111: 1665–72.
9. **Boman HG.** Antibacterial peptides: basic facts and emerging concepts. *J Intern Med.* 2003; 254: 197–215.
10. **Hunter HN, Jing W, Schibli DJ, *et al.*** The interactions of antimicrobial peptides derived from lysozyme with model membrane systems. *Biochim Biophys Acta.* 2005; 1668: 175–89.
11. **Jimenez MA, Evangelio JA, Aranda C, *et al.*** Helicity of alpha(404–451) and beta(394–445) tubulin C-terminal recombinant peptides. *Protein Sci.* 1999; 8: 788–99.
12. **Cho CH, Sung HK, Kim KT, *et al.*** COMP-angiopoietin-1 promotes wound healing through enhanced angiogenesis, lymphangiogenesis, and blood flow in a diabetic mouse model. *Proc Natl Acad Sci U S A.* 2006; 103: 4946–51.
13. **Nakagami H, Maeda K, Morishita R, *et al.*** Novel autologous cell therapy in ischemic limb disease through growth factor secretion by cultured adipose tissue-derived stromal cells. *Arterioscler Thromb Vasc Biol.* 2005; 25: 2542–7.
14. **Kunigiza Y, Tomita N, Taniyama Y, *et al.*** Acceleration of wound healing by combined gene therapy of hepatocyte growth factor and prostacyclin synthase with Shima jet. *Gene Ther.* 2006; 13: 1143–52.
15. **D'Andrea LD, Iaccarino G, Fattorusso R, *et al.*** Targeting angiogenesis: structural characterization and biological properties of a *de novo* engineered VEGF mimicking peptide. *Proc Natl Acad Sci U S A.* 2005; 102: 14215–20.
16. **Azuma J, Taniyama Y, Takeya Y, *et al.*** Angiogenic and antifibrotic actions of hepatocyte growth factor improve cardiac dysfunction in porcine ischemic cariomyopathy. *Gene Ther.* 2006; 13: 1206–13.
17. **Munoz V, Serrano L.** Elucidating the folding problem of helical peptides using empirical parameters. *Nat Struct Biol.* 1994; 1: 399–409.
18. **Petukhov M, Munoz V, Yumoto N, *et al.*** Position dependence of non-polar amino acid intrinsic helical propensities. *J Mol Biol.* 1998; 278: 279–89.
19. **Venyaminov S, Baikalov IA, Wu CS, *et al.*** Some problems of CD analyses of protein conformation. *Anal Biochem.* 1991; 198: 250–5.
20. **Yano K, Brown LF, Detmar M.** Control of hair growth and follicle size by VEGF-mediated angiogenesis. *J Clin Invest.* 2001; 107: 409–17.
21. **Zhang L, Falla TJ.** Antimicrobial peptides: therapeutic potential. *Expert Opin Pharmacother.* 2006; 7: 653–63.

Author Queries

Q1 Author: Please check authors' affiliations for correctness.
Q2 Author: Please provide manufacturer location for DAKO.

PDGFRα-positive cells in bone marrow are mobilized by high mobility group box 1 (HMGB1) to regenerate injured epithelia

Katsuto Tamai[a,1], Takehiko Yamazaki[a], Takenao Chino[a], Masaru Ishii[b], Satoru Otsuru[a], Yasushi Kikuchi[a], Shin Iinuma[a], Kotaro Saga[a], Keisuke Nimura[a], Takashi Shimbo[a], Noriko Umegaki[c], Ichiro Katayama[c], Jun-ichi Miyazaki[d], Junji Takeda[e], John A. McGrath[f], Jouni Uitto[g], and Yasufumi Kaneda[a,1]

[a]Division of Gene Therapy Science, and Departments of [c]Dermatology, [d]Nutrition and Physiological Chemistry, and [e]Environmental Medicine, Osaka University Graduate School of Medicine, Osaka 565-0871, Japan; [b]Laboratory of Biological Imaging, WPI-Immunology Frontier Research Center, Osaka University, Osaka 565-0871, Japan; [f]St. John's Institute of Dermatology, King's College London, Guy's Hospital, London SE1 9RT, United Kingdom; and [g]Department of Dermatology and Cutaneous Biology, Jefferson Medical College, Philadelphia, PA 19107

Edited by Darwin J. Prockop, Texas A&M Health Science Center, Temple, TX, and approved March 18, 2011 (received for review November 10, 2010)

The role of bone marrow cells in repairing ectodermal tissue, such as skin epidermis, is not clear. To explore this process further, this study examined a particular form of cutaneous repair, skin grafting. Grafting of full thickness wild-type mouse skin onto mice that had received a green fluorescent protein-bone marrow transplant after whole body irradiation led to an abundance of bone marrow-derived epithelial cells in follicular and interfollicular epidermis that persisted for at least 5 mo. The source of the epithelial progenitors was the nonhematopoietic, platelet-derived growth factor receptor α-positive (Lin⁻/PDGFRα⁺) bone marrow cell population. Skin grafts release high mobility group box 1 (HMGB1) in vitro and in vivo, which can mobilize the Lin⁻/PDGFRα⁺ cells from bone marrow to target the engrafted skin. These data provide unique insight into how skin grafts facilitate tissue repair and identify strategies germane to regenerative medicine for skin and, perhaps, other ectodermal defects or diseases.

epidermolysis bullosa | skin injury | stem cells | keratinocyte | tissue regeneration

Bone marrow (BM) cells contribute a substantial proportion of cells, both inflammatory and noninflammatory, that have roles in tissue homeostasis, repair, and regeneration. Such cells may be derived from either hematopoietic or mesenchymal stem cell populations, and subpopulations thereof can differentiate into both hematopoietic and mesenchymal lineage cells (for review, see refs. 1 and 2).

In skin, studies have shown that BM provides fibroblast-like cells in the dermis (of hematopoietic and mesenchymal lineages) and that the number of these cells increases after skin wounding (3, 4). BM can also generate epithelial cells, i.e., keratinocytes, in the epithelia, although the precise derivations and mechanisms to raise BM-derived keratinocytes are not fully known (3, 5–16). Human/mouse studies involving transplantation of sex-mismatched or genetically tagged BM cells have shown that keratin-positive bone marrow-derived cells can be found in skin epidermis, hair follicles, and sebaceous glands (6, 8, 9, 11, 12, 14, 16), sites that harbor skin stem cell niches (17). Moreover, in humans who have undergone BM transplantation (BMT), donor cells that have differentiated into keratinocytes can be detected in the epidermis for at least 3 y (8).

BM cells also contribute to skin development: Infusion of green fluorescent protein (GFP) BM cells in utero in mice leads to accumulation of a subpopulation of GFP-positive cells in nonwounded skin dermis, particularly in association with developing hair follicles (18). With regard to skin injury, both embryonic and postnatal transplantation of BM cells into mice lacking the skin protein, type VII collagen (Col 7) as well as postnatal studies in mice lacking type XVII collagen, basement membrane components that normally help secure adhesion between the epidermal and dermal skin layers, have demonstrated the capacity of BM to promote skin wound healing and to correct the intrinsic basement membrane defect (18–20). Most recently, a clinical trial of allogeneic whole BMT in humans lacking Col 7 (who have the inherited blistering skin disorder, recessive dystrophic epidermolysis bullosa, RDEB; OMIM226600) (21) has demonstrated that BM cells can repair fragile skin and restore Col 7 expression in skin basement membrane (22).

Collectively, however, these animal and human studies have shown that BM-derived keratinocytes are an extremely rare finding in the epidermis. Indeed, analyses in two different murine models have shown that BM-derived keratinocytes comprise only ≈0.0001–0.0003% of all keratinocytes in the new epidermis (13). The relative scarcity of such cells therefore raises questions about their biological significance. For example, it is not known whether these cells have a physiological role in epithelial regeneration and, if they do, under what circumstances? Moreover, it is not clear which particular cells in BM contribute to the epithelial repair. Furthermore, there is little awareness of the mechanism(s) through which the damaged epithelium signals to invoke mobilization and recruitment of the key BM cells. In this study, we have begun to address these questions, and here report identification of a specific subset of BM cells with epithelial differentiation potential as well as a unique in vivo mechanism through which these cells contribute to epithelial regeneration and maintenance.

Results

We first examined the contribution of BM-derived cells to epithelial regeneration in murine skin wounds. The wounds were created by using a scalpel and involved excision of a piece of full-thickness skin (i.e., including epidermis and dermis) thus creating an ulcer. The mice selected for wounding had received lethal dose irradiation followed by GFP-BMT, thereby allowing us to evaluate the contribution of GFP-BM cells to skin regeneration after injury (Fig. 1*A*). At 4 wk after the injury, GFP-positive keratinocytes were not obvious (Fig. 1*B*), indicating a minimal, if any, contribution of BM cells to epithelial regeneration, findings consistent with previous data (13). We then used the same

Author contributions: K.T. designed research; K.T., T.Y., T.C., M.I., S.O., Y. Kikuchi, S.I., K.S., K.N., T.S., and N.U. performed research; J.-i.M. and J.T. contributed new reagents/analytic tools; K.T., I.K., and Y. Kaneda analyzed data; and K.T., J.A.M., J.U., and Y. Kaneda wrote the paper.

Conflict of interest statement: K.T., T.Y., and Y. Kaneda have filed patents relating to the use of HMGB1 for bone marrow cell mobilization and recruitment to damaged tissue. These individuals also hold stock in Genomix plc, a bio-tech company involved in HMGB1 translational research.

This article is a PNAS Direct Submission.

Freely available online through the PNAS open access option.

[1]To whom correspondence may be addressed. E-mail: tamai@gts.med.osaka-u.ac.jp or kaneday@gts.med.osaka-u.ac.jp.

This article contains supporting information online at www.pnas.org/lookup/suppl/doi:10.1073/pnas.1016753108/-/DCSupplemental.

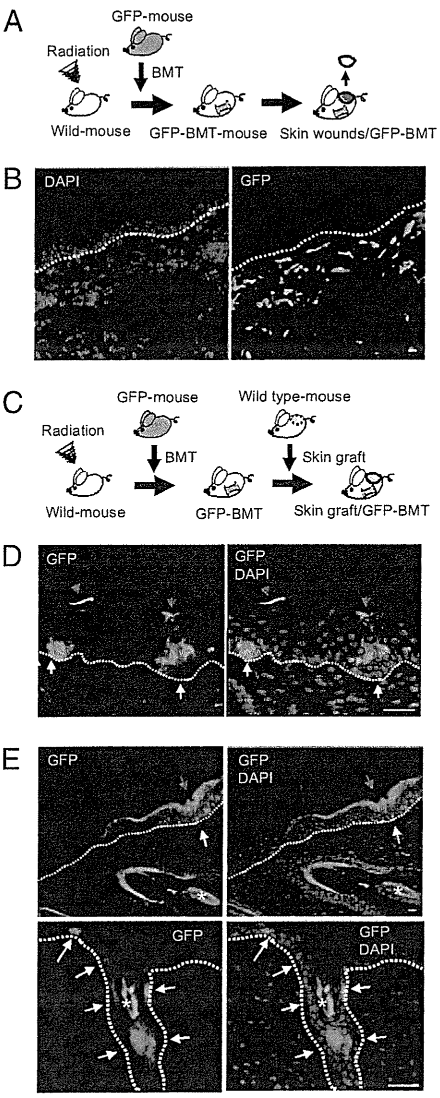

Fig. 1. BM-derived cells contribute to epidermal and follicular renewal in skin grafts, but not in skin wounds. (*A*) Schematic outlining details of the skin wound model on GFP-BMT mice. (*B*) Confocal-laser microscopy of skin sections from the reepithelialized wounds. Green fluorescence in the dermis represents BM-derived cells. Note that there is no GFP fluorescence within the regenerated epithelia. (*C*) Schematic outlining details of the skin engraftment of GFP-BMT mice. (*D*) Confocal-laser microscopy of skin sections from the 4-wk skin graft. Green fluorescence in the epidermis and the dermis represent BM-derived cells. Arrows indicate EPU-like structures that are composed of BM-derived epithelial cells emanating from the basal layer (white arrows) within the epidermis to the horny layer (red arrowheads). (*E*) Confocal-laser microscopy pictures of skin sections from the 5-mo skin graft. Green fluorescence in the epidermis, the hair follicles, and the dermis represent BM-derived cells. Arrows in *Upper* indicate sustained BM-derived epithelial cells emanating from the basal layer (white arrows) to the horny layer (red arrows). White arrows in *Lower* indicate sustained BM-derived follicular cells. Note that hair shafts show nonspecific auto-fluorescence (asterisks). White dotted lines indicate the dermal-epidermal and dermal-follicular junctions. (Scale bars: 50 μm.)

mouse model to examine a different form of skin repair, skin grafting, to further explore the potential contribution of BM cells (Fig. 1*C*). Surprisingly, we noted that significant numbers of GFP-positive cells expressing skin-specific keratin 5 formed epidermal proliferative unit (EPU)-like clusters in the epidermis of the skin graft in biopsies taken 4 wk after the engraftment (Fig. 1*D* and Fig. S1*A*). Furthermore, the BM-derived GFP-positive keratinocytes were maintained in the epidermis and hair follicles 5 mo after the engraftment (Fig. 1*E* and Fig. S1*B*). Given that mouse epidermis is renewed every 2–3 wk by epithelial stem cell-derived keratinocytes, those long-residing GFP BM-derived epithelial cells in the 5-mo-old graft are likely to contain epithelial progenitor/stem cells.

To assess whether the BM-derived epidermal cells might have functional significance, we then searched for BM-derived cells in the skin of Col 7-null mice engrafted onto the GFP-BMT mice (Fig. 2*A*). Because these mice have complete detachment of the epidermis after birth due to extensive skin and mucous membrane fragility (Fig. 2*A*) (23), we anticipated a potentially greater contribution of BM-derived cells in the regenerating epithelia of the engrafted Col 7-null mouse skin. The engrafted Col 7-null mouse skin initially showed extensive subepidermal detachment, similar to the skin pathology seen in human patients with RDEB (21). At 4 wk after the engraftment, we noted an even greater contribution of GFP-positive cells expressing keratinocyte-specific keratins in the regenerating epidermis and hair follicles of the engrafted Col 7-null mouse skin (Fig. 2 *B–D* and Fig. S2). Moreover, new Col 7 protein was present at the cutaneous basement membrane zone in the engrafted Col 7-null mouse skin (Fig. 2*E*). Notably, Col 7 labeling was maximal in the basement membrane adjacent to GFP-BM–derived epithelial cells. Evidence for BM-derived epithelial cells was further confirmed by demonstration of GFP-positive individual keratinocytes from the grafted skin by means of both flow cytometric analysis and cell culture (Fig. 2 *F* and *G*).

Collectively, these data showed that a subpopulation of BM cells contribute to epithelial regeneration and maintenance in these murine skin graft models. Analyses of sex chromatin numbers and fusion-dependent enhanced GFP expression in BM-derived epithelial cells in the grafted skin did not show any evidence for cell fusion, suggesting differentiation of the BM-derived cells as the likely mechanism for raising BM-derived keratinocytes in the skin graft (Figs. S3 and S4). Reverse wild-type BMT in a GFP mouse, followed by engrafting Col 7-null mouse skin onto the back of this mouse, excluded other possible extrinsic sources of keratinocytes in the skin graft besides the BM (Fig. S5).

We then investigated the subpopulation of BM cells that has the potential for epithelial differentiation. Recent studies have shown that the PDGFRα-positive nonhematopoietic BM cell population contains ectoderm-derived mesenchymal stem cells (MSCs) (24–26), indicating that perhaps PDGFRα$^+$ BM cells might be a putative source of BM-derived keratinocytes in the skin graft. To test this hypothesis, we examined BM from a heterozygous knock-in mouse in which a histone H2B-GFP fusion gene was inserted into the locus of the PDGFRα gene (PDGFRα-H2BGFP mouse); this knock-in results in accumulation of GFP fluorescence within the nuclei of PDGFRα-expressing cells. We found that the PDGFRα$^+$ BM cells were exclusively enriched in the Lineage-negative (Lin$^-$) cell population from the knock-in mouse BM (Fig. S6) and that the Lin$^-$ population provided proliferating PDGFRα$^+$ fibroblastic cells in culture (Fig. 3*A*). Lin$^-$ indicates negativity for the cell surface antigens CD5, B220, CD11b, Gr-1, 7–4, and Ter-119 and excludes mature hematopoietic cells, such as T cells, B cells, monocytes/macrophages, granulocytes, and erythrocytes/their committed precursors from BM. Flow cytometric analysis indicated that the Lin$^-$ and PDGFRα$^+$ (Lin$^-$/PDGFRα$^+$) cells were independent from the Lin$^-$/c-kit$^+$ cell population, which includes a hematopoietic stem cell pool (Lin$^-$/c-kit$^+$/Sca-1$^+$) in BM (Fig. 3*B* and Fig. S7). We found that Lin$^-$ cell populations collectively accounted for ≈5.6% of the total number of BM cells (Fig. 3*B*). The Lin$^-$/PDGFRα$^-$/c-kit$^+$ and Lin$^-$/PDGFRα$^-$/c-kit$^-$ BM cells comprised ≈2.28% and ≈3.11% of total BM cells, respectively. We observed that the Lin$^-$/PDGFRα$^+$ BM cells (≈0.22% of the total BM cells) could exclusively generate BM-derived epithelial cells expressing keratin 5 in culture after supplementation with skin soaked buffer (SSB),

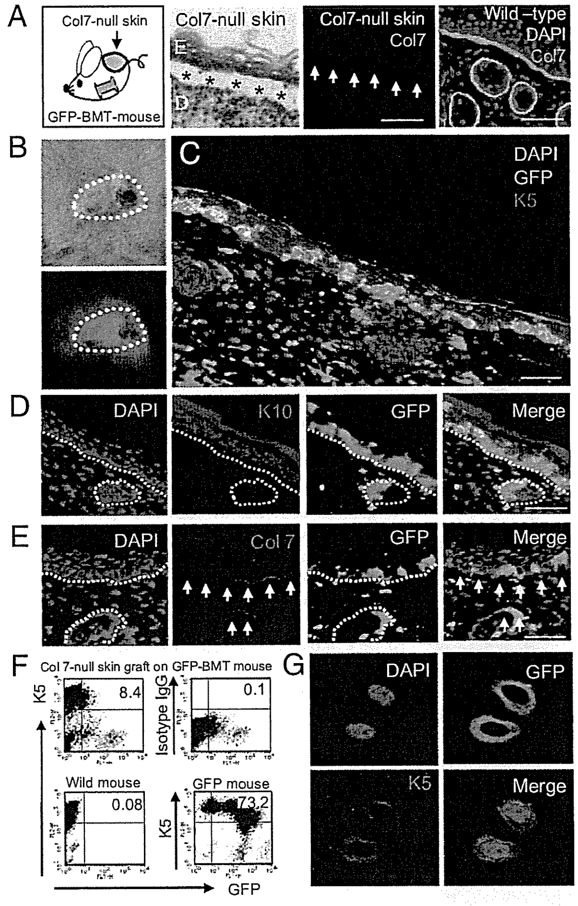

Fig. 2. BM cells substantially contribute to the repair of grafted Col 7-null epidermis. (*A*) Schematic picture of the Col 7-null skin engraftment on GFP-BMT mice (*Left*); hematoxylin-eosin staining of Col 7-null mouse skin (*Left Center*). Asterisks indicate separation of the epidermis (*E*) from the dermis (*D*); Col 7 immunostaining in the Col 7-null skin (*Right Center*). (*Right*) Arrows indicate dermal-epidermal junction, Col 7 staining of wild-type mouse skin. Green color indicates Col 7 staining. (*B*) Accumulation of GFP fluorescence (*Lower*) within the region of the Col 7-null skin graft (*Upper*). The white dotted line indicates the margins of the skin graft. (*C* and *D*) Confocal-laser microscopy pictures of sections from the Col 7-null mouse skin that had been surgically grafted. Blue color indicates DAPI staining. Green fluorescence in the epidermis and the dermis represents BM-derived cells. Red labeling indicates keratin 5 (K5; *C*) or keratin 10 (K10; *D*) immunofluorescence. Yellow color image represents BM-derived cells that express both GFP (green) and K5 (red; *C*) or K10 (red; *D*). (*E*) Col 7 expression in grafted Col 7-null mouse skin. White dotted lines indicate dermal-epidermal and dermal-follicular junctions. White arrows indicate immunofluorescence for Col 7 (red) at the basement membrane zone. (Scale bars: 50 μm.) (*F*) Flow cytometric analysis for K5 and GFP in the epidermal cell suspension of Col 7-null skin engrafted onto a GFP-BMT mouse (*Upper Left*), wild-type mouse skin (*Lower Left*), and the GFP-transgenic mouse skin (*Lower Right*). *Upper Right* shows isotype control for K5 in the epidermis of the grafted Col 7-null skin. (*G*) Confocal-laser micrographs of cultured BM-derived epithelial cells isolated from the epidermis of the Col 7-null skin graft labeled with GFP or K5.

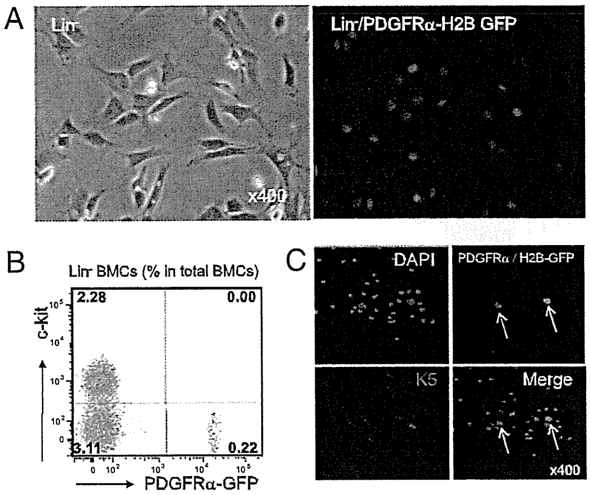

Fig. 3. Characterization of BM cells of the PDGFRα knock-in mouse demonstrates that PDGFRα$^+$ subpopulation give rise to epithelial progenitors. (*A*) Phase-contrast (*Left*) and GFP-fluorescent (*Right*) micrographs of the Lin$^-$ BM cells in culture. All adherent and proliferating Lin$^-$ cells were positive with PDGFRα-GFP labeling in their nuclei. (*B*) Flow cytometry analysis for PDGFRα-GFP and c-kit expression on the Lin$^-$ cells in total BM cells of the PDGFRα knock-in mice. The number (%) in the chart represents the population of each fraction in the total number of BM cells. Note that there is no population in the PDGFRα-positive and c-kit-positive fraction (upper right corner) in BM. (*C*) Confocal-laser micrographs of cultured bone marrow cells (BMCs) from a heterozygous knock-in mouse with a histone H2B-GFP fusion gene inserted into the PDGFRα gene locus. PDGFRα promoter-dependent H2B-GFP expression was noted by accumulation of GFP fluorescence in the nuclei (PDGFRα/H2B-GFP, indicated by white arrows; *Upper Right*) of cells expressing K5 (*Lower Left*).

in which excised newborn mouse skin had been soaked in phosphate buffer saline (PBS) for 24 h (Fig. 3*C* and Fig. S8). The Lin$^-$/PDGFRα$^-$ cell population also contained adherent and proliferative cells in culture, but none of these cells showed differentiation into keratin 5-positive keratinocytes with SSB supplementation (Fig. S8). These data suggest that the BM-derived keratinocytes are not of hematopoietic origin, but instead are derived from a specific subpopulation of Lin$^-$/PDGFRα$^+$ BM cells. In this context, additional flow cytometry analysis of the Lin$^-$/PDGFRα$^+$ BM cells did not show expression of CD146 or CD271 (Fig. S9), both of which are established markers of human BM MSCs (27), indicating different cell surface molecule profiles for human BM MSCs and mouse Lin$^-$/PDGFRα$^+$ BM cells.

We then investigated the mechanism through which the transplanted skin graft is able to recruit Lin$^-$/PDGFRα$^+$ cells from the BM. First, we established a Boyden chamber migration assay to demonstrate that Lin$^-$/PDGFRα$^+$ BM cells migrate toward one or more chemoattractants in SSB (Fig. 4*A*). We then assessed which molecules in the SSB have the capacity to induce migration of Lin$^-$/PDGFRα$^+$ BM cells. We noted that a heparin-binding fraction of SSB was able to induce robust migration of the Lin$^-$/PDGFRα$^+$ BM cells (Fig. 4*B*). This finding supports the notion that the excised skin graft can release heparin-binding molecules capable of attracting these particular BM cells. To find the precise molecules involved, we fractionated SSB by heparin-affinity chromatography and obtained several fractions with strong activity for inducing Lin$^-$/PDGFRα$^+$ BM cell migration (Fig. S10). Some fractions had strong cell-migrating activity but comparatively less protein expression: These fractions were then subjected to SDS/PAGE analysis (Fig. 4*C*). Three prominent silver-stained proteins were observed in the gel, which were then further analyzed by liquid chromatography/tandem mass spectrometry. They were identified as nucleolin, anti-thrombin III (AT-III), and high mobility group box 1 (HMGB1) (Fig. 4*C*). Nucleolin is a eukaryotic nucleolar phosphoprotein that is involved in the synthesis and maturation of ribosomes in nucleoli (28). AT-III is a well-characterized anticoagulant molecule generated in the liver, and which exists in blood plasma (29). HMGB1, also known as amphoterin, is a nuclear protein that can regulate chromatin structure and gene expression (30). It is also released from necrotic cells and some apoptotic cells and acts

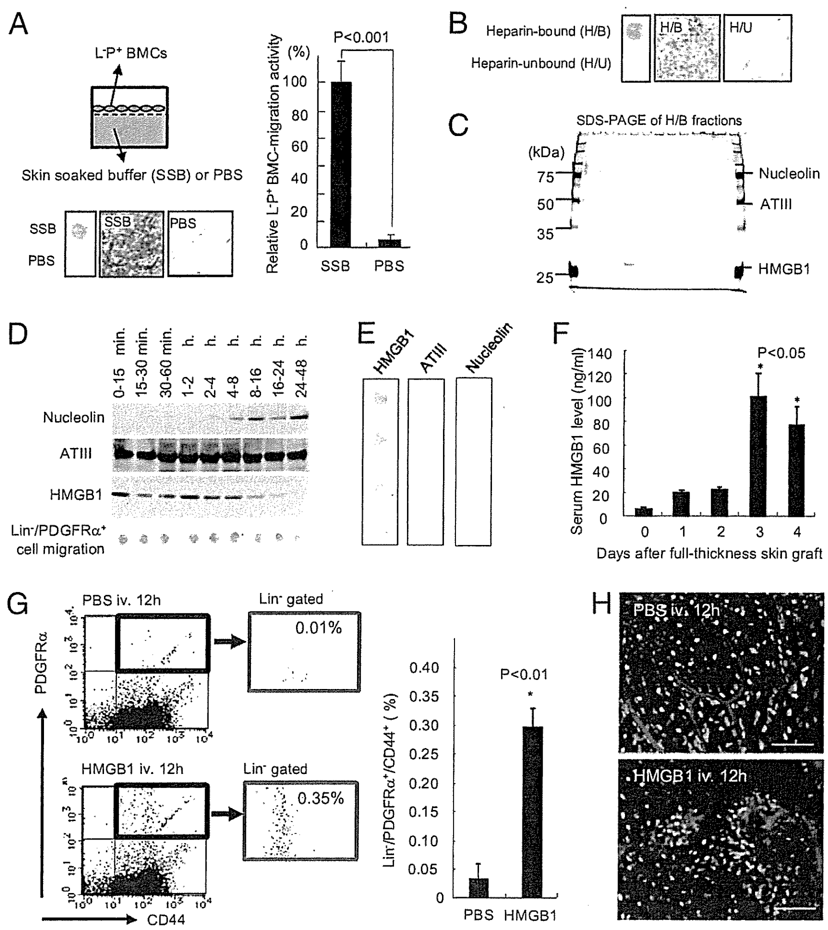

Fig. 4. Elevation of HMGB1 in serum is induced by skin grafting and mobilizes Lin$^-$/PDGFRα^+ cells from BM. (*A*) Schematic illustration of the Boyden chamber approach to assess migration of the Lin$^-$/PDGFRα^+ cells to SSB or PBS. The actual and relative migration of these cells to both buffers is shown. (*B*) Assessment of Lin$^-$/PDGFRα^+ cells migration to heparin-bound (H/B) or unbound (H/U) fractions of the SSB. (*C*) SDS/PAGE of H/B SSB fractions with Lin$^-$/PDGFRα^+ cell migration activity. Results of liquid chromatography-tandem mass spectrometry for three major proteins in the gel are noted on the right. (*D*) Western blot against nucleolin, AT-III, and HMGB1 in the SSB obtained at sequential time periods. The lowest blot shows Lin$^-$/PDGFRα^+ cell migration activities in each SSB. (*E*) Lin$^-$/PDGFRα^+ cell migration assay in a Boyden chamber with recombinant HMGB1, AT-III, and nucleolin. (*F*) HMGB1 levels in mouse sera after full-thickness skin grafting with newborn wild-type mouse skin. Asterisks (*) indicate statistical significance vs. Day 0 ($P < 0.05$, $n = 4$). (*G*) Flow cytometric analyses of Lin$^-$/PDGFRα^+/CD44$^+$ cells of peripheral blood mononuclear cells of mice 12 h after systemic administration of HMGB1 (10 μg in 400 μL of PBS) or PBS (400 μL). Asterisk (*) represents statistical significance ($P < 0.01$, $n = 4$). (*H*) Intravital two-photon imaging of the calvaria BM in PDGFRα-H2BGFP mice 12 h after systemic administration of PBS (400 μL; *Left*) or HMGB1 (10 μg in 400 μL of PBS; *Right*) via the tail vein. Green color, GFP expressed under the promoter of PDGFRα; red color, BM microvasculature visualized by i.v. injection of 70-kDa dextran-conjugated Texas Red. (Scale bar: 50 μm.)

as an inflammatory regulator. Other studies, however, have indicated that HMGB1 may also act as a local chemo-attractant for various hematopoietic and nonhematopoietic cells that can regulate tissue remodeling (31).

The next objective was to determine the time course for release of the proteins from excised skin graft into the buffer (Fig. 4*D*). Of note, both HMGB1 and AT-III were rapidly released within a few minutes into the SSB fraction that demonstrated strong chemoattractant activity for Lin$^-$/PDGFRα^+ BM cells. AT-III secretion continued at similar levels for at least 48 h, whereas HMGB1 release gradually declined after ≈8 h—a time course that paralleled the chemoattraction findings. With regard to nucleolin, its presence in the SSB only started 2 h after incubation, possibly reflecting the consequences of necrosis in the excised skin. To evaluate the chemoattractant properties, we expressed mouse HMGB1 in HEK293 cells and compared the in vitro activity of the purified recombinant protein to induce Lin$^-$/PDGFRα^+ BM cell migration. Recombinant AT-III and nucleolin were also assessed, but cell migration assays demonstrated that only HMGB1 could induce migration of these particular BM cells (Fig. 4*E*). We also explored the nature of the receptor on Lin$^-$/PDGFRα^+ BM cells relevant to the cell migration and excluded a role for two known receptors that can mediate the extracellular cytokine effects of HMGB1, the receptor for advanced glycation endproduct (RAGE) and toll-like receptor (TLR) 4 (32–34) (see *SI Results and Discussion* and Fig. S11 for details).

Next, we explored the source of HMGB1 in the grafted skin. Immunofluorescent microscopy analysis of HMGB1 protein in the skin graft showed abundant staining in the epidermis and much less in the dermis, reflecting the higher cellularity in the epidermis (Fig. S12). We then analyzed Col 7-null mouse skin for HMGB1 release and noted that the detached epithelia (blister roofs) released significant amounts of HMGB1 after soaking in PBS (Fig. S13 *A* and *B*). These observations suggest that the epithelial tissue in the skin graft could be a significant source of HMGB1 in vivo. Further support for damaged epithelium as a source of HMGB1 was demonstrated by finding elevated HMGB1 in freshly generated subepidermal blister fluid of human subjects with RDEB ($n = 3$) (Fig. S13*C*). We then investigated the systemic effects of HMGB1 after skin injury. We first measured HMGB1 levels in the sera of mice that had received a skin graft of wild-type newborn mouse skin (Fig. 4*F*). We observed a marked increase in HMGB1 serum levels 3 d after grafting. Of note, however, no increase in serum HMGB1 was noted in mice with full thickness wounds but no skin graft (Fig. S13*D*), suggesting that the transplanted epithelial tissue is likely to be the source of the elevated HMGB1 in the sera. We also detected ≈60-fold higher levels of HMGB1 in the sera of individuals with RDEB ($n = 3$) compared with similarly aged normal control subjects ($n = 3$) (Fig. S13*E*). These observations led us to hypothesize that systemic elevation of HMGB1 in the blood might positively induce recruitment of Lin$^-$/PDGFRα^+ cells from BM to raise BM-derived keratinocytes (as well as fibroblasts) in the regenerating injured skin, and that this might be one mechanism through which the practice of skin grafting achieves its clinical goals.

To confirm this hypothesis, we systemically administered recombinant HMGB1 at levels similar to that seen in the sera of skin grafted mice to wild-type mice. We observed that this action could mobilize Lin$^-$/PDGFRα^+ BM cells into the blood circulation (Fig. 4*G*). Lower doses of HMGB1 failed to mobilize these cells (Fig. S14). We noted no local or systemic inflammation or other potentially adverse effects in the mice, despite the high doses of systemic HMGB1 administered (Fig. S15). To further investigate the mechanics of this mobilization by HMGB1 in vivo, we performed intravital two-photon imaging of calvaria BM in living PDGFRα-H2BGFP mice. This experiment showed that HMGB1 could mobilize PDGFRα-positive cells, allowing them to congregate around blood vessels and, thereby, allow egress into the circulation in vivo (Fig. 4*H*).

To confirm that the mobilized BM-derived PDGFRα$^+$ circulating cells provide the epithelial cells in vivo, we combined FACS-sorted PDGFRα$^+$/GFP$^+$ BM cells with wild-type PDGFRα$^-$ BM cells and transplanted these cells to lethally irradiated mice, which then received skin grafts of Col 7-null mouse skin (Fig. 5*A*). Very few cells were GFP-positive in the peripheral blood mononuclear cell populations of the PDGFRα$^+$/GFP$^+$ BM transplanted mice (Fig. 5*B*). However, those GFP-positive circulating cells that originated from the transplanted PDGFRα$^+$ BM cells had adherent and proliferative capacities in culture (Fig. 5*B*). Four weeks after the Col 7-null skin engraftment, multiple foci of GFP-positive cells expressing keratin 5 were observed in the epithelia of the engrafted skin (Fig. 5*C*), suggesting that the BM-derived PDGFRα$^+$ circulating cells contain a population that can differentiate into epithelial cells in the skin graft.

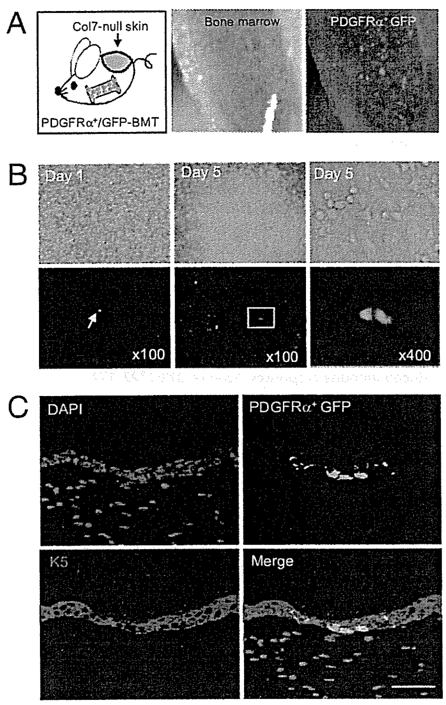

Fig. 5. Mobilized Lin$^-$/PDGFRα$^+$ BM-derived cells in circulation contribute to epithelial regeneration of the skin graft in vivo. (*A*) Schematic illustration showing Col 7-null skin graft on a mouse transplanted with PDGFRα-positive/GFP-BM cells (*Left*); bright field (*Center*) and dark field (*Right*) stereomicroscopic pictures of femoral BM in a PDGFRα$^+$/GFP-BMT mouse. Green fluorescence indicates PDGFRα$^+$/GFP-BM cells. (*B*) Bright field (*Upper*) and dark field (*Lower*) fluorescent microscopic pictures of cultured peripheral blood mononuclear cells that were obtained from the PDGFRα$^+$/GFP-BMT mouse engrafted with Col 7-null skin. (*Left*) A single PDGFRα$^+$/GFP-BM-derived cell in culture (Day 1). (*Center*) Proliferation of the single PDGFRα$^+$/GFP-BM-derived cell in culture (Day 5). (*Right*) Dividing adherent cells indicated in the white lined box in *Lower Center*. (*C*) Confocal-laser microscopic pictures of a section of grafted Col7-null skin onto a PDGFRα$^+$/GFP-BMT mouse. GFP fluorescence was merged with the red immunofluorescence of K5 to provide the yellow color. DAPI staining (*Upper Left*), GFP fluorescence (*Upper Right*), K5 staining (*Lower Left*), and a merged image (*Lower Right*). (Scale bar: 50 μm.)

Discussion

This work clearly demonstrates that Lin$^-$/PDGFRα$^+$ cells from BM significantly contribute to the regeneration of the epidermis after skin grafting in vivo, and that one biological repair mechanism involves the key cells being mobilized in response to elevated HMGB1 levels in serum, the source of which is the skin graft. The observation that tissue damage can recruit BM stromal cells for tissue repair is well-established (35), but here we have defined a subpopulation of cells that have the capacity to repair skin, including epidermis. The Lin$^-$/PDGFRα$^+$ BM cell marker profile is not unique to one particular cell population, and our data suggest that it is shared by ≈1 in 450 BM cells. PDGFRα is not expressed by hematopoietic stem cells but by MSCs in bone marrow that can give rise to mesenchymal lineage cells as well as neuroepithelial and neural crest lineage cells (24–26), suggesting that the Lin$^-$/PDGFRα$^+$ BM cells contain an MSC fraction (discussed further in *SI Results and Discussion*).

Our study has shown that in situations in which there is significant damage to the epidermis, such as Col 7 deficiency leading to subepidermal blistering, at least some of the Lin$^-$/PDGFRα$^+$ cells have the plasticity to become BM-derived epithelial progenitors, to generate and sustain new keratinocytes, and to correct the intrinsic lack of Col 7. Moreover, we have identified HMGB1 as a specific factor involved in Lin$^-$/PDGFRα$^+$ BM cell responses. Our data indicate that HMGB1, which is rapidly released from the detached or blistered Col 7-deficient epithelia, can mobilize Lin$^-$/PDGFRα$^+$ BM cells into the circulation and accelerate regeneration of the skin by recruiting these cells to raise BM-derived epithelial cells and BM-derived mesenchymal cells in the epidermis and dermis of Col 7-null skin, respectively.

HMGB1 is a highly conserved, abundant, and ubiquitously expressed 30-kDa nonhistone protein with diverse biologic functions (36, 37). With regards to human and murine HMGB1, only 2 of 215 amino acids show species differences (>99% identical) and both reside in the C-terminal region outside of the known receptor- and DNA-binding motifs (38, 39). HMGB1 can act as a mobile and dynamic nucleo-cytoplasmic protein influencing multiple processes in chromatin such as transcription, replication, recombination, and DNA repair (39, 40), but HMGB1 can also be secreted into the extracellular milieu as a signaling molecule when cells are stressed (41). HMGB1 can bind exogenous and endogenous agents such as endotoxin, microbial DNA, and nucleosomes, and induces adaptive and innate immune responses via TLR2/4/9 followed by NF-κB activation (42, 43), contributing to inflammation, autoimmune dysregulation, and carcinogenesis. However, purified recombinant HMGB1 has little, if any, proinflammatory activity (44). Indeed, free HMGB1, that is unbound to endogenous/exogenous inflammatory factors, is able to suppress inflammatory reactions in noninjured tissues by inhibiting TLR-mediated NF-κB signaling (33). Biologically, HMGB1 can be regarded as a critical factor for maintaining tissue homeostasis in cleaning damaged/infected tissues (i.e., promoting intralesional inflammation), but also in protecting surrounding noninjured tissues (i.e., suppressing inflammation), and accelerating regeneration of damaged tissues by mobilizing and recruiting specific BM cells, that include epithelial progenitors when there is extensive epithelial injury, such as in Col 7-deficient RDEB skin.

The concept that a particular threshold concentration of HMGB1 in serum is relevant to mobilizing Lin$^-$/PDGFRα$^+$ BM cells and targeting them to damaged tissue also offers unique possibilities to augment a variety of other tissue repair mechanisms. It is likely that, in several other situations, systemic administration of HMGB1 to achieve serum levels similar to those observed in RDEB could be used as a therapeutic strategy to recruit stem/progenitor cells to accelerate regeneration of damaged tissue. Precisely which tissues might benefit from HMGB1-induced mobilization of Lin$^-$/PDGFRα$^+$ BM cells remains to be determined. What has also not been determined thus far are the dynamics of both the release of the Lin$^-$/PDGFRα$^+$ cells from the BM and the events that promote recruitment and migration within the target tissue and the other potential local microenvironmentinduced and biochemical processes that contribute to improved wound healing (35) (discussed further in *SI Materials and Methods*). Nevertheless, we believe our data represent a significant advance in identifying a direction for potentially bringing stem/progenitor cell regenerative medicine to a broader clinical arena.

Materials and Methods

BMT. BM cells were isolated under sterile conditions from 8- to 10-wk-old male C57BL/6 transgenic mice that ubiquitously expressed enhanced green fluorescent protein (GFP). Recipients were 8- to 10-wk-old female C57BL/6 mice that were lethally irradiated with 10 Gy of X-rays, and each irradiated recipient received 5×10^6 BM cells from GFP transgenic mice kindly provided by Masaru Okabe (Osaka University). Experiments were performed on the BMT mice at least 6 wk after the BMT.

Mouse Skin Transplantation. Full-thickness skin from wild-type and Col 7-null newborn mice (graft size $\approx 2 \times 2$ cm) was carefully isolated by excision after the mice had been euthanized under systemic anesthesia, and engrafted onto the backs of the GFP-BMT mice, wild-type BMT mice, and K5-Cre-GFP-BMT mice, with grafting just above the muscular fascia.

Immunofluorescent Microscopy Analysis. The engrafted skins were removed, fixed with 2% paraformaldehyde, and subjected to immunofluorescent analysis. The excised skins were embedded in Tissue-Tec OCT Compound (Sakura Finetek), frozen on dry ice, and stored at −20 °C. For immunofluorescence staining, 6-μm-thick sections were labeled with rabbit polyclonal anti-mouse antibodies. Subsequently, sections were stained with goat anti-rabbit IgG secondary antibody.

Cell-Migration Assay. Chemokinetic migration of $Lin^-/PDGFR\alpha^+$ cells was assayed by using a modified Boyden chamber. In brief, 1.0 μg of HMGB1 in 27 μL of DMEM was added in the lower chambers, and 10^6 cells/mL of $Lin^-/PDGFR\alpha^+$ cells suspended in 50 μL of DMEM containing 10% FBS were added to the upper chamber. The cells on the lower side of the membrane were stained with Diff-Quick (Sysmex).

ACKNOWLEDGMENTS. This work was supported by the following grants: a grant from the Northern Osaka (Saito) Biomedical Knowledge-Based Cluster Creation Project; Special Coordination Funds for Promoting Science and a Grant-in-Aid for Scientific Research from the Ministry of Education, Culture, Sports, Science and Technology of Japan; and a Health and Labour Sciences Research Grant (Research of Intractable Diseases) from the Ministry of Health, Labour and Welfare of Japan.

1. Orkin SH, Zon LI (2008) Hematopoiesis: An evolving paradigm for stem cell biology. *Cell* 132:631–644.
2. Prockop DJ (2009) Repair of tissues by adult stem/progenitor cells (MSCs): Controversies, myths, and changing paradigms. *Mol Ther* 17:939–946.
3. Fathke C, et al. (2004) Contribution of bone marrow-derived cells to skin: Collagen deposition and wound repair. *Stem Cells* 22:812–822.
4. Ishii G, et al. (2005) In vivo characterization of bone marrow-derived fibroblasts recruited into fibrotic lesions. *Stem Cells* 23:699–706.
5. Wu Y, Zhao RC, Tredget EE (2010) Concise review: Bone marrow-derived stem/progenitor cells in cutaneous repair and regeneration. *Stem Cells* 28:905–915.
6. Krause DS, et al. (2001) Multi-organ, multi-lineage engraftment by a single bone marrow-derived stem cell. *Cell* 105:369–377.
7. Hematti P, et al. (2002) Absence of donor-derived keratinocyte stem cells in skin tissues cultured from patients after mobilized peripheral blood hematopoietic stem cell transplantation. *Exp Hematol* 30:943–949.
8. Körbling M, et al. (2002) Hepatocytes and epithelial cells of donor origin in recipients of peripheral-blood stem cells. *N Engl J Med* 346:738–746.
9. Badiavas EV, Falanga V (2003) Treatment of chronic wounds with bone marrow-derived cells. *Arch Dermatol* 139:510–516.
10. Badiavas EV, Abedi M, Butmarc J, Falanga V, Quesenberry P (2003) Participation of bone marrow derived cells in cutaneous wound healing. *J Cell Physiol* 196:245–250.
11. Kataoka K, et al. (2003) Participation of adult mouse bone marrow cells in reconstitution of skin. *Am J Pathol* 163:1227–1231.
12. Borue X, et al. (2004) Bone marrow-derived cells contribute to epithelial engraftment during wound healing. *Am J Pathol* 165:1767–1772.
13. Fan Q, et al. (2006) Bone marrow-derived keratinocytes are not detected in normal skin and only rarely detected in wounded skin in two different murine models. *Exp Hematol* 34:672–679.
14. Inokuma D, et al. (2006) CTACK/CCL27 accelerates skin regeneration via accumulation of bone marrow-derived keratinocytes. *Stem Cells* 24:2810–2816.
15. Rovó A, Gratwohl A (2008) Plasticity after allogeneic hematopoietic stem cell transplantation. *Biol Chem* 389:825–836.
16. Sasaki M, et al. (2008) Mesenchymal stem cells are recruited into wounded skin and contribute to wound repair by transdifferentiation into multiple skin cell type. *J Immunol* 180:2581–2587.
17. Fuchs E, Horsley V (2008) More than one way to skin . . .. *Genes Dev* 22:976–985.
18. Chino T, et al. (2008) Bone marrow cell transfer into fetal circulation can ameliorate genetic skin diseases by providing fibroblasts to the skin and inducing immune tolerance. *Am J Pathol* 173:803–814.
19. Tolar J, et al. (2009) Amelioration of epidermolysis bullosa by transfer of wild-type bone marrow cells. *Blood* 113:1167–1174.
20. Fujita Y, et al. (2010) Bone marrow transplantation restores epidermal basement membrane protein expression and rescues epidermolysis bullosa model mice. *Proc Natl Acad Sci USA* 107:14345–14350.
21. Fine JD, et al. (2008) The classification of inherited epidermolysis bullosa (EB): Report of the Third International Consensus Meeting on Diagnosis and Classification of EB. *J Am Acad Dermatol* 58:931–950.
22. Wagner JE, et al. (2010) Bone marrow transplantation for recessive dystrophic epidermolysis bullosa. *N Engl J Med* 363:629–639, and erratum (2010) 363:1383.
23. Heinonen S, et al. (1999) Targeted inactivation of the type VII collagen gene (Col7a1) in mice results in severe blistering phenotype: A model for recessive dystrophic epidermolysis bullosa. *J Cell Sci* 112:3641–3648.
24. Takashima Y, et al. (2007) Neuroepithelial cells supply an initial transient wave of MSC differentiation. *Cell* 129:1377–1388.
25. Morikawa S, et al. (2009) Prospective identification, isolation, and systemic transplantation of multipotent mesenchymal stem cells in murine bone marrow. *J Exp Med* 206:2483–2496.
26. Morikawa S, et al. (2009) Development of mesenchymal stem cells partially originate from the neural crest. *Biochem Biophys Res Commun* 379:1114–1119.
27. Bühring HJ, et al. (2009) Phenotypic characterization of distinct human bone marrow-derived MSC subsets. *Ann N Y Acad Sci* 1176:124–134.
28. Mongelard F, Bouvet P (2007) Nucleolin: A multiFACeTed protein. *Trends Cell Biol* 17: 80–86.
29. Quinsey NS, Greedy AL, Bottomley SP, Whisstock JC, Pike RN (2004) Antithrombin: In control of coagulation. *Int J Biochem Cell Biol* 36:386–389.
30. Harris HE, Raucci A (2006) Alarmin(g) news about danger: Workshop on innate danger signals and HMGB1. *EMBO Rep* 7:774–778.
31. Palumbo R, Bianchi ME (2004) High mobility group box 1 protein, a cue for stem cell recruitment. *Biochem Pharmacol* 68:1165–1170.
32. Riuzzi F, Sorci G, Donato R (2006) The amphoterin (HMGB1)/receptor for advanced glycation end products (RAGE) pair modulates myoblast proliferation, apoptosis, adhesiveness, migration, and invasiveness. Functional inactivation of RAGE in L6 myoblasts results in tumor formation in vivo. *J Biol Chem* 281:8242–8253.
33. Chen GY, Tang J, Zheng P, Liu Y (2009) CD24 and Siglec-10 selectively repress tissue damage-induced immune responses. *Science* 323:1722–1725.
34. Maroso M, et al. (2010) Toll-like receptor 4 and high-mobility group box-1 are involved in ictogenesis and can be targeted to reduce seizures. *Nat Med* 16:413–419.
35. Phinney DG, Prockop DJ (2007) Concise review: Mesenchymal stem/multipotent stromal cells: the state of transdifferentiation and modes of tissue repair—current views. *Stem Cells* 25:2896–2902.
36. Rauvala H, Rouhiainen A (2010) Physiological and pathophysiological outcomes of the interactions of HMGB1 with cell surface receptors. *Biochim Biophys Acta* 1799: 164–170.
37. Sims GP, Rowe DC, Rietdijk ST, Herbst R, Coyle AJ (2010) HMGB1 and RAGE in inflammation and cancer. *Annu Rev Immunol* 28:367–388.
38. Baxevanis AD, Landsman D (1995) The HMG-1 box protein family: Classification and functional relationships. *Nucleic Acids Res* 23:1604–1613.
39. Stros M (2010) HMGB proteins: Interactions with DNA and chromatin. *Biochim Biophys Acta* 1799:101–113.
40. Liu Y, Prasad R, Wilson SH (2010) HMGB1: Roles in base excision repair and related function. *Biochim Biophys Acta* 1799:119–130.
41. Wang H, et al. (1999) HMG-1 as a late mediator of endotoxin lethality in mice. *Science* 285:248–251.
42. Campana L, Bosurgi L, Bianchi ME, Manfredi AA, Rovere-Querini P (2009) Requirement of HMGB1 for stromal cell-derived factor-1/CXCL12-dependent migration of macrophages and dendritic cells. *J Leukoc Biol* 86:609–615.
43. Yanai H, et al. (2009) HMGB proteins function as universal sentinels for nucleic-acid-mediated innate immune responses. *Nature* 462:99–103.
44. Kazama H, et al. (2008) Induction of immunological tolerance by apoptotic cells requires caspase-dependent oxidation of high-mobility group box-1 protein. *Immunity* 29:21–32.

CED
Clinical and Experimental Dermatology

The course of pregnancy and childbirth in three mothers with recessive dystrophic epidermolysis bullosa

T. Hanafusa, K. Tamai,* N. Umegaki, Y. Yamaguchi,† S. Fukuda,‡ Y. Nishikawa,§ N. Yaegashi,¶ R. Okuyama, J. A. McGrath†† and I. Katayama**

*Department of Dermatology and *Stem Cell Therapy Science, Osaka University Graduate School of Medicine, Osaka, Japan; †Department of Geriatric and Environmental Dermatology, Nagoya City University Graduate School of Medical Sciences, Nagoya, Japan; ‡Department of Obstetrics and Gynecology, Maizuru Kyosai Hospital, Kyoto, Japan; §Department of Obstetrics and Gynecology, Kizawa Memorial Hospital, Gifu, Japan; ¶Department of Gynecology and Obstetrics, Tohoku University Graduate School of Medicine, Miyagi, Japan; **Department of Dermatology, Shinshu University School of Medicine, Nagano, Japan; and ††St John's Institute of Dermatology, King's College London, Guy's Hospital, London, UK*

doi:10.1111/j.1365-2230.2011.04179.x

Summary

Background. Recessive dystrophic epidermolysis bullosa (RDEB) is an autosomal recessive skin disease caused by mutations in the type VII collagen gene (*COL7A1*), resulting in detachment of the entire epidermis due to loss or hypoplasticity of the anchoring fibrils that normally secure the basement membrane to the underlying dermis. Trauma-induced blistering is often complicated by chronic erosions and scarring. From that perspective, pregnancy in RDEB might be considered an indication for elective caesarean section in a bid to minimize perineal blistering. To date, only four cases of pregnancy and delivery in patients with RDEB have been reported.

Cases. We report three more women, each with RDEB-generalized other (RDEB-GO), all of whom had successful vaginal deliveries without major cutaneous or mucosal complications. One woman also had a second child, by vaginal delivery, indicating a lack of vaginal stenosis after the first birth.

Conclusions. These cases show that RDEB-GO is not an absolute primary indication for elective caesarean section and that, perhaps surprisingly, genital/perineal blistering and scarring are not inevitable consequences of childbirth. Moreover, breastfeeding is also feasible in women with RDEB-GO.

Introduction

Epidermolysis bullosa (EB) comprises a heterogeneous group of inherited blistering skin diseases with widely varying degrees of severity.[1] Recessive dystrophic (RD)EB is an autosomal recessive disease producing severe blistering beneath the lamina densa of the dermoepidermal junction. It is caused by mutations on both alleles of the *COL7A1* gene, resulting in structural defects of the anchoring fibrils that normally secure the basement membrane to the underlying dermis.[2–4]

Severe generalized RDEB (RDEB-SG), which was previously known as the Hallopeau–Siemens type of RDEB, is generally caused by a combination of premature termination codon mutations resulting from nonsense, frameshift or splice-site mutations on both *COL7A1* alleles. These mutations lead to either nonsense-mediated decay of the mRNA, or to truncated polypeptides that are unable to assemble into functional anchoring fibrils. Less severe forms of RDEB, called RDEB-generalized other (RDEB-GO), are often caused by compound heterozygous mutations such as one premature termination codon mutation and one missense mutation. As a result, full-length type VII collagen

Correspondence: Dr Katsuto Tamai, Division of Gene Therapy Science, Osaka University Graduate School of Medicine, 2-2 Yamadaoka, Suita city, Osaka 565-0871, Japan
E-mail: tamai@gts.med.osaka-u.ac.jp

Conflict of interest: none declared.

Accepted for publication 8 May 2011

polypeptides can be synthesized from the allele with the missense mutation, but the substituted amino acid affects the stabilization of the anchoring fibrils by disulfide bonding, or results in other structural changes.[4–6]

Because the skin fragility in RDEB is often followed by delayed wound healing and scarring, pregnant women with RDEB (or their carers) may be concerned about vaginal delivery because of the possibility of severe genital blistering and scar formation. However, caesarean section is not a straightforward alternative in patients with RDEB because there may be erosions on the back that interfere with spinal anaesthesia, or blisters/scarring in the mouth and upper airway that compromise the safety or practicality of general anaesthesia. Guidelines for best practice and indeed sensible advice for the management of pregnancy and childbirth in RDEB are currently lacking. Moreover, only three previously published reports have addressed pregnancy and delivery in RDEB.[1,2,7] We report three further women with RDEB who had safe pregnancies and vaginal deliveries.

Case reports

All three patients were Japanese, and all had been monitored since birth. All three had generalized cutaneous blisters and scars at sites of minimal trauma that had occurred since birth. Their fingers had adhered to each other, resulting in pseudosyndactyly. Their nails were deformed and some nail plates were lost.

Patient 1

This patient had cutaneous blisters present from birth, and over the years, many generalized cutaneous blisters, erosions, ulcers and scars had developed as a result of gentle mechanical trauma (Figs 1a,b). The molecular diagnosis of RDEB-GO was based on the detection of two compound heterozygous *COL7A1* mutations, c.8644G>A (p.Glu2882Lys) and c.8569G>T (p.Glu2857X), resulting in abnormal type VII collagen production. The first mutation is a missense mutation inherited from the patient's mother, and the second is a nonsense mutation inherited from her father.

The patient became pregnant at the age of 30 years. Pregnancy was confirmed by ultrasonography examination, and during gestation, there were no major complications or abnormalities related to the pregnancy. After 36 weeks and 6 days of gestation, the patient was admitted because of severe general fatigue and inability to manage her skin lesions by herself at home. She had no genital mucosal ulcers, but the number of skin ulcers around her lower abdomen had increased as it became distended in pregnancy.

On admission, the patient had a poor appetite and she had not been gaining weight during the latter part of her pregnancy. Laboratory investigations revealed the following: haemoglobin 9.0 g/dL (normal range 12.0–15.0 g/dL), albumin 2.5 g/dL (3.6–4.7 g/dL), cholinesterase 1018 U/L (2700–5600 U/L), total cholesterol 105 mg/dL (150–220 mg/dL), iron 30 mg/dL (41–127 mg/dL), prothrombin international normalized

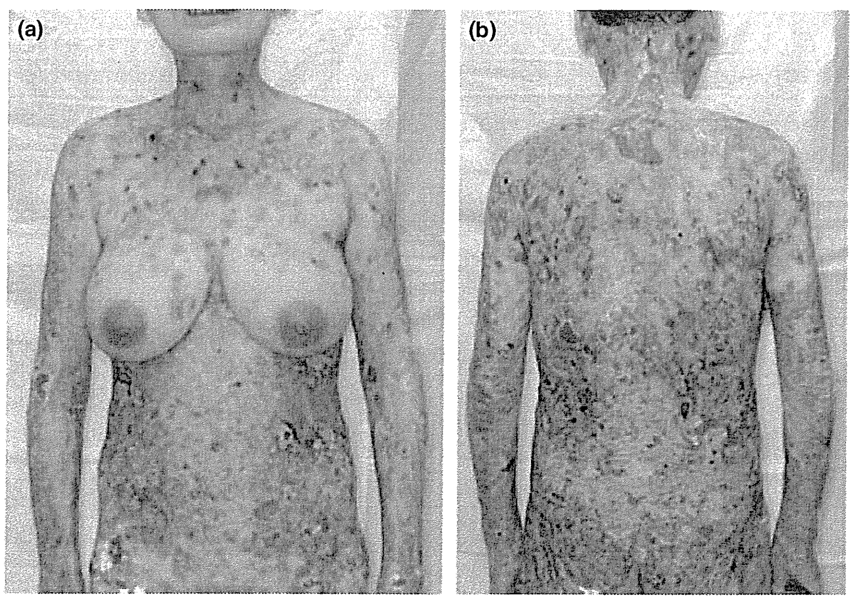

Figure 1 Patient 1. Several days after delivery: (a) anterior and (b) posterior views showing extensive cutaneous blisters.

ratio 1.35 (0.85–1.15), white cell count 7040/mm^3 (3300–9400/mm^3), C-reactive protein 4.6 mg/dL (≤ 0.2 mg/dL), and platelets 34.5×10^4/mm^3 ($13.0–32.0 \times 10^4$/mm^3). The patient's Birmingham Epidemolysis Bullosa Severity (BEBS) score was 19.0.[8] Nevertheless, the growth of the fetus was normal.

On the estimated date of delivery (full term), the patient delivered a healthy boy by vaginal delivery with episiotomy. The baby was 2508 g (−1.6 SD) in weight, and had no signs of EB on his skin or mucous membranes.

The mother did not develop any major cutaneous or vaginal ulcers, and the total course of her delivery was similar to that of a woman without RDEB. The episiotomized perineum healed normally, and there was no stenosis of the patient's vagina. We advised her not to breastfeed the baby because his suckling might have caused new blisters on her breasts. The mother had no aftereffects of delivery, and the child developed normally.

Patient 2

The second patient had many generalized cutaneous blisters present since birth (Fig. 2), and the clinical diagnosis of RDEB-GO was confirmed by detection of compound heterozygous *COL7A1* mutations, c.7741G>A (p. Gly2581Arg) and c.8329C>T (p. Arg2777X), resulting in abnormal type VII collagen production.

The patient was 27 years old when she became pregnant, which was confirmed by ultrasonography examination. She had no genital mucosal ulcers, but she was admitted to our hospital for 2 weeks at 19 weeks gestation because of severe lower abdominal pain induced by a threatened miscarriage. However, the symptoms abated after bed rest and administration of ritodrine and cefotiam. The growth of the fetus was normal. The patient was admitted to our hospital at 38 weeks and 5 days of gestation in preparation for delivery. Her BEBS score was 11.6.

On the estimated date of delivery, labour pains started, and on the next day, a healthy boy, 2884 g in weight, was delivered vaginally after episiotomy. Significant bleeding accompanied the delivery, which almost induced hypovolaemic shock, but which settled after rapid infusion of intravenous fluids.

The mother's episiotomized perineum healed normally and there was no stenosis of her vagina. As there were no skin blisters around the breast, we encouraged her to breastfeed her baby. Breastfeeding was not associated with blistering of the nipples or areolae; she continued breastfeeding for 3 months and the baby developed normally.

Two years later, in 2002, the patient became pregnant for the second time. In week 27 of gestation, mild anaemia was detected, with haemoglobin levels of 9.9 g/dL. Intravenous administration of iron maintained the patient's haemoglobin levels. No significant genital mucosal lesions or scar-induced stenosis were noted before the birth, and the growth of the fetus was normal. On the estimated date of delivery, the patient was admitted to our hospital, and a healthy girl weighing 3108 g was delivered vaginally after episiotomy. The patient did not develop any major cutaneous or vaginal erosions or scarring during the subsequent follow-up period she breastfed her second baby for 3 months as well.

Figure 2 Patient 2. Abdomen with extensive blistering at the time the patient's first pregnancy was confirmed.

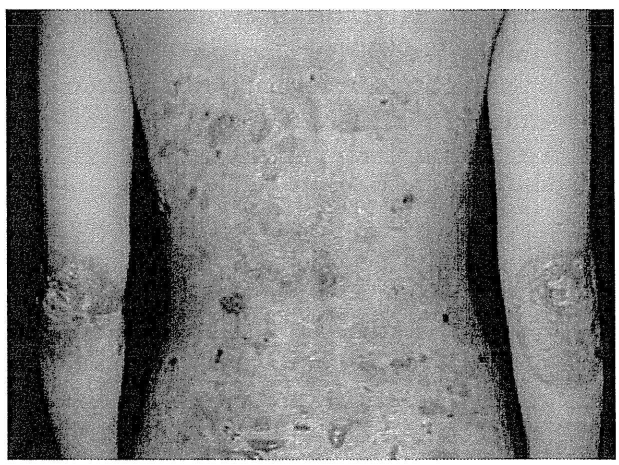

Figure 3 Patient 3. Posterior view taken 3 years after delivery; no cutaneous adverse events were seen.

Table 1 Summary of RDEB pregnancies.

Ref.	Phenotype	Genotype	Complications	Delivery method	Adverse events
Bianca *et al.*[1]	RDEB-SG	c.8441-14del21	Genital mucous lesions, fetal growth retardation, premature rupture of membranes	Caesarean	Blistering around caesarean scar
Baloch *et al.*[2]	RDEB	Unknown	None	Vaginal	None
	RDEB	Unknown	Strong fear of vaginal delivery	Caesarean	None
Buscher *et al.*[7]	RDEB-SG	Unknown	Mild anaemia, polyhydramnios	Vaginal (twice)	None
Present study					
Patient 1	RDEB-GO	c.8644G>A and c.8569G>T	Severe general fatigue, moderate anaemia	Vaginal	None
Patient 2	RDEB-GO	c.7741G>A and c.8329C>T			
First delivery			Threatened spontaneous abortion	Vaginal	Much bleeding
Second delivery			Slight anaemia	Vaginal	None
Patient 3	RDEB-GO	Unknown	Moderate anaemia, HCV carrier	Vaginal	None

HCV, hepatitis C virus; RDEB, recessive dystrophic epidermolysis bullosa; RDEB-SG, RDEB-severe generalized; RDEB-GO, RDEB-generalized other.

Patient 3

The third patient also had many generalized cutaneous blisters since birth (Fig. 3), and had been diagnosed with RDEB-GO based on her clinical and skin biopsy findings but without genetic testing. She was a carrier of the hepatitis C virus.

At the age of 21 years, pregnancy was confirmed by ultrasonography examination. The number of skin ulcers around patient's lower abdomen increased during the pregnancy, but no genital mucosal ulcers occurred; however, she was admitted to hospital for several weeks to treat the skin ulcers. She was found to have moderate anaemia, with a haemoglobin level of 9.0 g/dL at 10 weeks of gestation, and received an iron preparation. Her BEBS score was 12.5. and the growth of the fetus was normal.

At 39 weeks and 6 days, a 2996 g healthy boy was delivered vaginally. The baby had no signs of EB on his skin or mucous membranes. The patient did not develop any major cutaneous or vaginal ulcers, and there was no scarring noted in subsequent follow-up. In this case, we recommended avoidance of breastfeeding because of skin ulceration and pain around the nipple.

Discussion

We report three women with RDEB-GO who each had successful vaginal delivery to give birth to healthy children who had no signs of skin fragility. Of note, all three women were engaged in sexually active relationships, emphasizing that this form of mechanobullous disease is not necessarily an impediment to regular vaginal intercourse. As shown in the summary of RDEB pregnancies, including our cases reported here (Table 1), caesarean section was selected only in two previously reported cases, because of presence of genital blistering or a strong fear of the potential complications that might follow vaginal delivery. Surprisingly, however, for those women who underwent vaginal delivery, there were no major adverse sequelae such as vaginal stenosis, even in an individual with RDEB-SG,[7] suggesting that the genital mucosa in RDEB can withstand vaginal delivery.

In general, caesarean section may be indicated for pregnant women with a history of previous caesarean section or dystocia, or in cases of fetal distress or breech presentation. It may also be indicated for women with placenta praevia, severe pre-eclampsia, eclampsia or active genital herpes simplex virus infection.[9] Medical considerations for caesarean section may also include heart failure, which could be relevant in RDEB, as the disease can be associated with dilated cardiomyopathy, and therefore careful assessment of cardiac function is advisable.[10] None of our three patients had any general obstetric indications for caesarean section, although all presented with slight or moderate iron-deficiency anaemia, a common complication in RDEB.[11] Heart function was assessed and deemed normal in all cases, and none presented with any local contraindication to vaginal delivery such as any pre-existing genital mucosal ulcers or blisters. Taken together, our three cases suggest that vaginal delivery can occur safely in patients with RDEB in the absence of any other obstetric or medical contraindications or concerns.

Another possible issue for mothers with RDEB is whether breastfeeding is appropriate, given the possibility of inducing significant blistering.[7] However, our second patient breast-fed without adverse consequences, suggesting that it may not be necessary to avoid breastfeeding if there are no pre-existing skin lesions around the breasts or nipples.

Conclusion

We report three cases of successful vaginal delivery for childbirth in pregnant mothers with RDEB-GO. Although further cases will add to the clinical experience and help refine the advice, our observations indicate that pregnancy, vaginal delivery and breastfeeding are not specifically associated with major problems or sequelae in women with RDEB-GO.

References

1 Bianca S, Reale A, Ettore G. Pregnancy and cesarean delivery in a patient with dystrophic epidermolysis bullosa. *Eur J Obstet Gynecol Reprod Biol* 2003; **110**: 235–6.

2 Baloch MS, Fitzwilliams B, Mellerio J *et al.* Anaesthetic management of two different modes of delivery in patients with dystrophic epidermolysis bullosa. *Int J Obstet Anesth* 2008; **17**: 153–8.

3 Tamai K, Hashimoto I, Hanada K *et al.* Japanese guidelines for diagnosis and treatment of junctional and dystrophic epidermolysis bullosa. *Arch Dermatol Res* 2003; **295** (Suppl. 1): S24–8.

4 Dang N, Murrell DF. Mutation analysis and characterization of COL7A1 mutations in dystrophic epidermolysis bullosa. *Exp Dermatol* 2008; **17**: 553–68.

5 Fine JD, Eady RA, Bauer EA *et al.* The classification of inherited epidermolysis bullosa (EB): report of the Third International Consensus Meeting on Diagnosis and Classification of EB. *J Am Acad Dermatol* 2008; **58**: 931–50.

6 Christiano AM, Anhalt G, Gibbons S *et al.* Premature termination codons in the type VII collagen gene (COL7A1) underlie severe, mutilating recessive dystrophic epidermolysis bullosa. *Genomics* 1994; **21**: 160–8.

7 Buscher U, Wessel J, Anton-Lamprecht I *et al.* Pregnancy and delivery in a patient with mutilating dystrophic epidermolysis bullosa (Hallopeau-Siemens type). *Obstet Gynecol* 1997; **89**: 817–20.

8 Moss C, Wong A, Davies P. The Birmingham Epidermolysis Bullosa Severity score: development and validation. *Br J Dermatol* 2009; **160**: 1057–65.

9 Cunningham FG, Williams JW. *Williams Obstetrics*, 23rd edn. New York: McGraw-Hill Medical, 2010.

10 Oh SW, Lee JS, Kim MY *et al.* Recessive dystrophic epidermolysis bullosa associated with dilated cardiomyopathy. *Br J Dermatol* 2007; **157**: 610–12.

11 Atherton DJ, Cox I, Hann I. Intravenous iron (III) hydroxide-sucrose complex for anaemia in epidermolysis bullosa. *Br J Dermatol* 1999; **140**: 773.

 http://dx.doi.org/10.5021/ad.2011.23.S3.S408

CASE REPORT

Morphea on the Breast after a Needle Biopsy

Noriko Arase, M.D., Ph.D., Ken Igawa, M.D., Ph.D., Satoko Senda, M.D., Mika Terao, M.D., Ph.D., Hiroyuki Murota, M.D., Ph.D., Ichiro Katayama, M.D., Ph.D.

Department of Dermatology, Graduate School of Medicine, Osaka University, Osaka, Japan

Localized scleroderma (morphea) usually develops spontaneously, but the precise mechanisms underlying disease development are obscure. However, a significant number of cases suggest that morphea is induced by external stimuli. Herein, we report a case of morphea that developed after a needle biopsy. **(Ann Dermatol 23(S3) S408~S410, 2011)**

-Keywords-
Morphea, Needle biopsy

INTRODUCTION

Localized scleroderma (morphea) usually develops spontaneously. However, a significant number of reports suggest that external stimuli can induce morphea. Although trauma is reported as a morphea trigger, the mechanism has remained unclear. Herein, we report a case of morphea that developed after a needle biopsy and discuss the mechanisms underlying these phenomena.

CASE REPORT

A 35-year-old Japanese female noticed a small breast tumor and underwent a needle biopsy examination. Three months later, she found an egg-sized, slightly itchy erythema on her left breast, around the needle biopsy scar. Subsequently, two walnut-sized erythemas developed. A topical steroid was ineffective. Within a few months, the erythema inflammatory reaction gradually attenuated but sclerotic plaques with slight pigmentation remained. A similar progressing sclerotic plaque had also developed on her right upper arm. She was referred to our hospital with the complaint of these sclerotic plaques.

A physical examination revealed an oval sclerotic plaque and two small round sclerotic plaques on her left inner breast (Fig. 1A). An oval sclerotic plaque was observed on her upper right arm (Fig. 1B). No physical findings relevant to systemic sclerosis such as Raynaud's phenomenon, sclerodactyly, or internal organ dysfunction was observed.

A histopathological examination of the biopsy specimen from the sclerotic lesion on the upper arm showed a thickened reticular dermis consisting of closely packed, homogenous collagen bundles. A significant number of mononuclear cells had infiltrated the lower dermis (Fig. 1C). Alpha-smooth muscle actin-positive cells had increased significantly in the lower dermis (Fig. 1D). Laboratory data including various auto-antibodies were normal. From these findings, the patient was diagnosed with morphea developing after a needle biopsy.

This patient was successfully treated with oral administration of both suplatast tosilate and tranilast, as well as topical tretinoin tocoferil. Six months later, the first sclerotic lesion on the left inner breast had improved. Other sclerotic lesions on her breast and right arm had completely disappeared.

DISCUSSION

Several studies have suggested that morphea begins with unidentified antigens interacting with the host immune system. Both endogenous and exogenous factors cited previously may influence the disease. Several external stimuli participate in morphea pathogenesis , including trauma or operative stress[1], irradiation[2,3], infections (viral

Received January 13, 2011, Revised August 5, 2011, Accepted for publication August 8, 2011

Corresponding author: Ken Igawa, M.D., Ph.D., Department of Dermatology, Graduate School of Medicine, Osaka University, Yamada-oka 2-2, Suita city, Osaka 565-0871, Japan. Tel: 81-6-6879-3031, Fax: 81-6-6879-3039, E-mail: igawa@derma.med.osaka-u.ac.jp